

Estimates of Lightning NO_x Production based on High Resolution OMI NO₂ Retrievals over the Continental US

Response to Anonymous Referee #1

Xin Zhang, Yan Yin, Ronald van der A, Jeff L. Lapierre, Qian Chen,
Xiang Kuang, Shuqi Yan, Jinghua Chen, Chuan He and Rulin Shi

March 8, 2020

We thank the reviewer for his/her positive comments and very careful reading of the main article. The individual corrections suggested are addressed below. The reviewer's comments will be shown in **red**, our response in **blue**, and changes made to the paper are shown in **black** block quotes. Unless otherwise indicated, page and line numbers correspond to the original paper. Figures, tables, or equations referenced as "Rn" are numbered within this response; if these are used in the changes to the paper, they will be replaced with the proper number in the final paper.

1) L31-37: Is there a difference between the IFLUX approach and IFLUX proxy?

Why does the IFLUX approach predict a 15% decrease in lightning while the IFLUX proxy predicts a 3.4% / K increase in lightning over the CONUS?

Sorry for the misleading. IFLUX approach is as same as IFLUX proxy. These two values are relative to different regions. 15% decrease is for global lightning while 3.4% / K is limited to the CONUS.

While **global lightning** is predicted to increase by 5 — 16% over the next century with the CTH approach (Clark et al., 2017; Banerjee et al., 2014; Krause et al., 2014), a 15% decrease in **global lightning** was estimated with IFLUX in 2100 under a strong global warming scenario (Finney et al., 2018).

2) L31-37: How are water mass fluxes related to lightning amounts?

Thanks for pointing this out. As illustrated in the IFLUX method, the lightning amounts are directly related to ice mass flux, although Romps (2019) mentioned that these condensates are ultimately derive from the condensation of water vapor. We have rewritten this sentence.

They reported that higher CAPE and updraft velocities caused by global warming could lead to the large increases in tropical lightning simulated by CAPE × P proxy, while IFLUX proxy predicts little change in tropical lightning because of the small changes in **the mass flux of ice**.

3) L60: are low → were low

Fixed.

But they found LNO_x production to be highly variable and correlations between flash rate densities and LNO_x production **were** low in some cases.

4) L79: by subtracting temporal average → by subtracting the temporal average

Fixed.

The tropospheric NO_x background was removed by subtracting **the** temporal average of NO_x at each box where the value was weighted by the number of OMI pixels which meet the optical cloud pressure and CRF criteria required to be considered deep convection but has 1 flash or less instead.

5) L154-156: I am confused by the sentence beginning with "Although the simulated total flash densities ...".

I would suggest the following for lines 154 – 155.

→ simulated total flash densities are higher than observed by ENTLN over the Southeast US and lower than observed in the North Central US (Fig 2). The impact of these biases on LNO_x production is discussed and mitigated in sections 3.1 and 3.4.

Thanks for your suggestion. Improved.

Simulated total flash densities are higher than ENTLN observations over the Southeast US and lower than observations in the North Central US (Fig. 2). The impact of these biases on LNO_x production is discussed and mitigated in Sect. 3.1 and 3.4.

6) L164: for freshly produced lightning → to freshly produced lightning

Fixed.

The concept of AMF_{LNO_x} was also used in Beirle et al. (2009) to investigate the sensitivity of satellite instruments **to** freshly produced lightning NO_x.

7) L177: Hence, the tropospheric → Hence, much of the tropospheric

Fixed.

Hence, **much of** the tropospheric NO₂ measured by OMI lies inside the cloud rather than above the cloud top.

8) L180: compositions → composition

L180: fraction the NO₂ → fraction of the NO₂

Fixed.

The sensitivity study of Beirle et al. (2009) compared the chemical **composition** from the cloud bottom to the cloud top and revealed that a significant fraction **of** the NO₂ within the cloud originating from lightning can be detected by the satellite.

9) L195–198: Is it possible to compare the 50 grid box minimum with the 3–5 pixel minima?

If no, I would not mention the later minima. If yes, please explain how they relate.

50 grid boxes are approximately equal to 3–5 pixels. We have decided to remove the later minima which may confuse readers.

10) L210-211: You need to state why you continue to use a relatively high flash threshold when it induces a low-bias. What are the advantages of your threshold?

The possible low-bias of your approach begs the question of what the PE would be if you changed your threshold to 1 flash box⁻¹ from 2400 flash box⁻¹.

Can this calculation be made with limited effort. If yes, do so. If no, explain why it is not appropriate to use a low threshold.

There are some reasons why we prefer the relatively higher threshold and we have added the explanation in Sect. 2.5.

According to your advice, we have also checked the 1 flash box⁻¹ condition which is applied to both ENTLN and WRF lightning data and added to the Appendix B.

2.5: Procedures for Deriving LNO_x

... Since our study focuses on developing a new AMF and compare results with other works using the similar lightning thresholds (Lapierre et al., 2020; Pickering et al., 2016), we will only discuss results based on the strict criteria in the main texts. For comparisons between 2400 flashes box⁻¹ criterion and 1 flash box⁻¹ criterion, scatter diagrams using different lightning criteria are presented in Appendix .

Appendix B: LNO_x Production based on Lower Lightning Thresholds

While we used 2400 flashes box⁻¹ and 8160 strokes box⁻¹ per 2.4 hour time window for detecting LNO_x, here we show results obtained when using 1 flash box⁻¹ and 3.4 strokes box⁻¹ in the same time window. We note that the WRF total lightning threshold is also reduced to 1 flash box⁻¹, but we keep the ratio condition unchanged. Briefly, the condition is CRF90_ENTLN1(3.4)_TL1_ratio50 as shown in Table 1.

Similarly, the order of estimated daily PEs is LNO₂Clean > LNO₂ > NO₂Vis > LNO₂Vis (Fig. B1 [see Fig. R1]). Compared with Fig. 4, the LNO₂ per flash and LNO_x per flash are larger while PEs based on stroke data are smaller. Considering the additional boxes of fewer lightning counts, differences in the daily mean flashes and NO_x results in different PEs and the relationship presents more like the power function as mentioned in Bucselá et al. (2019).

Instead of using the nonlinear regression of power function:

$$y = \alpha x^\beta \quad (1)$$

where x is flashes or strokes and y is NO₂ or NO_x, we take the logarithm of both sides and apply the linear regression to data:

$$\log_{10} y = \log_{10} \alpha + \beta \log_{10} x \quad (2)$$

As expected, the linear regression based on logarithmized data performs better in this situation and yields $\alpha = 38$ kmol, and $\beta = 0.3$ for LNO_x per flash (Fig. B2 [see Fig. R2]). Since we use the unbinned data (flashes not divided into many groups), we compare our results with Bucselá et al. (2019) based on the same kind of data ($\alpha = 10.3$ kmol, and $\beta = 0.42$). The large difference of α is related to the method of estimating LNO_x, different lightning data and different regions. Note that the resolution (13×24 km²) of OMI could weaken the signal of LNO_x. We believe the phenomenon of higher production efficiency as flash rate decreases (Fig. B3 [see Fig. R3]) could be explored in much detail with higher resolution data like the TROPOMI data.

11) L216: has a LNO_x → has an LNO_x

Fixed.

The ratio $\geq 50\%$ indicates that more than half of the NO_x above the cloud must has an LNO_x source.

12) L235: condition of ratio > 50% → condition of more than half of the above-cloud NO_x having an LNO_x source.

Fixed.

The result is almost the same as that under the CRF90_ENTLN_TL1000 condition which is without **the condition of more than half of the above-cloud NO_x having an LNO_x source.**

13) L240 needs to be included as part of the previous paragraph.

Moved.

14) L240-244: The substantial decrease in PE as the CRF threshold is increased from 90 to 100% is somewhat concerning and not well explained.

You hint that this is likely due to the decrease in valid days. Please explain this more clearly.

This is caused by the higher lightning density with fewer LNO_x (Fig. R4). We have added it.

When the CRF increases from 90% to 100%, the LNO_x PE decreases because of the higher lightning density with fewer LNO_x (not shown). The increment of LNO_x PE caused by the CRF increase from 70% to 90% is opposite to the result of Pickering et al. (2016).

15) L300: Improvement of our approach with respect to what?

We have made it more clear.

With respect to the LNO₂ production, the patterns in Fig. 6 indicate the improvement of our approach is different in polluted and clean regions.

16) L308: I don't understand this statement: "Generally, the profiles of background NO₂ ratio are C-shape because LNO₂ concentrations are higher than background NO₂ in the UT".

Wouldn't high NO₂ concentrations result in lower background ratios?

The UT is mostly located between the OMI detected cloud pressure (lower black horizontal line, Fig. 7) and tropopause (higher black horizontal line, Fig. 7). The trough of C-shape profile of background ratio ($[\text{NO}_2 - \text{LNO}_2]/\text{NO}_2$) is due to the higher LNO₂ concentrations than background NO₂ there.

Generally, the profiles of **the ratio of background NO₂ over total NO₂** are C-shape because **UT LNO₂** concentrations are higher than **UT background NO₂** concentrations.

17) L316: convections over → convective cases over

Fixed.

As a result, our approach is less sensitive to background NO₂ and more suitable for **convective cases** over polluted locations.

18) L321: The largest relative change is 153.8% among the six grids where the highest clouds occur. Is this what you mean? → The largest change in PE due to changes in methodology (153.8%) occurs at New Orleans, which has the lowest cloud pressure and consequently the smallest visible column.

Yes, you are right. We have rewritten the sentence according to your suggestion.

The largest relative change (153.8%) occurs at New Orleans, which has the lowest cloud pressure and consequently the smallest visible column.

19) L333: concentrations is larger → concentrations are larger

Fixed.

Because updrafts are stronger and flash rates are higher in anomalous storms, UT LNO_x concentrations **are** larger in anomalous than normal polarity storms.

20) L361: "Fortunately, the AMFs and estimated LNO₂ change little in that region".

Is this a fortuitous coincidence or is this because the profile shape is relatively insensitive to the magnitude of LNO_x PE?

This is caused by the relatively insensitive to the magnitude of LNO_x PE, because the flash density could affect the value of AMF. We have made it clearer after the sentence.

Because the Southeast U.S. has the highest flash density (Fig. 2), the NO₂ in the numerator of AMF is dominated by LNO₂. Both the SCD and VCD will increase when the model uses higher LNO₂. In other words, the sensitivity to the LNO setting decreases and the relative distribution of LNO₂ matters.

21) L392: Wasn't 0.46 their mean AMF and not their total sensitivity?

Yes, 0.46 is the mean AMF which is named sensitivity in their paper.

Note that we have used another method to estimate the uncertainty caused by CP (See *No. 1, Response to Reviewer #3*).

22) L431: Is 20% an uncertainty or a bias?

Thanks for the correction, that is a bias. We have recalculated the uncertainty using the bias (See *No. 1, Response to Reviewer #3*).

We assign a **20% bias with ± 15% uncertainty** to this error considering the possible positive NO₂ measurements interferences (Allen et al., 2019; Bucselo et al., 2019) and **estimate the uncertainty to be 15% for LNO_x PE**.

23) L448: → 100 – 250 mol per flash which is higher than but overlaps with our estimate

Fixed.

Bucselo et al. (2010) estimated LNO_x PE of 100 – 250 mol/flash **which is higher than but overlaps with our estimate**.

24) L449: 80 mol per flash is not 50% smaller than your estimate of 90 mol per flash.

Please rephrased based on your updated values.

The linear regression in Pickering et al. (2016) is based on daily summed NO_x and flashes. We used this method before and switched to daily mean values now. As a result, it is better to compare with their results using the same method. We have pointed this special background below:

Pickering et al. (2016) estimated LNO_x PE to be 80 ± 45 mol per flash for the Gulf of Mexico. This is 50% smaller than our flash-based results over the CONUS, **if we use the same linear regression method which is based on the daily summed values instead of daily mean values.**

25) L464: Add sentence supporting your assertion that this method has reduced the sensitivity to background NO₂. Presumably, using information from section 3.3.

L466: Unclear, if the method of Pickering et al. overestimates PE due to over-cloud background NO₂ in polluted regions as they do an "after-the-fact" 18% adjustment to the PE to account for background pollution.

The reduce of the sensitivity to background NO₂ is inferred from the comparison between our results and others. We have rewritten these conclusions to make them clearer.

Compared with Lapierre et al. (2020), we find that the LNO₂ production could be larger when the below-cloud LNO₂ is taken into account, especially for the high clouds. Meanwhile, if the method of Pickering et al. (2016) is applied without the background NO₂ correction, the derived LNO_x production efficiency is similar to ours in clean regions or regions with high LNO₂ concentration above the cloud, but it could be overestimated more than 18% in polluted regions.

27) L468: "we find that the larger production model settings lead to larger retrieval of LNO_x ..." Be clear as to how important this finding is. How large a bias is induced by the larger production settings?

Fixed.

Finally, implementing profiles generated with different model settings of lightning (1×200 mol NO flash⁻¹ and 2×500 mol NO flash⁻¹), we find that the larger LNO production setting leads to **62% larger retrieval of LNO_x on average** despite some regionally dependent effects caused by the nonlinear calculation of AMF.

References

- Allen, D. J., Pickering, K. E., Bucsela, E. J., Krotkov, N., and Holzworth, R.: Lightning NO_x Production in the Tropics as Determined Using OMI NO₂ Retrievals and WWLLN Stroke Data, *Journal of Geophysical Research: Atmospheres*, <https://doi.org/10.1029/2018JD029824>, 2019.
- Banerjee, A., Archibald, A. T., Maycock, A. C., Telford, P., Abraham, N. L., Yang, X., Braesicke, P., and Pyle, J. A.: Lightning NO_x, a key chemistry–climate interaction: impacts of future climate change and consequences for tropospheric oxidising capacity, *Atmospheric Chemistry and Physics*, 14, 9871–9881, <https://doi.org/10.5194/acp-14-9871-2014>, 2014.
- Beirle, S., Salzmann, M., Lawrence, M. G., and Wagner, T.: Sensitivity of satellite observations for freshly produced lightning NO_x, *Atmospheric Chemistry and Physics*, 9, 1077–1094, <https://doi.org/10.5194/acp-9-1077-2009>, 2009.
- Bucsela, E. J., Pickering, K. E., Huntemann, T. L., Cohen, R. C., Perring, A., Gleason, J. F., Blakeslee, R. J., Albrecht, R. I., Holzworth, R., Cipriani, J. P., Vargas-Navarro, D., Mora-Segura, I., Pacheco-Hernández, A., and Laporte-Molina, S.: Lightning-generated NO_x seen by the Ozone Monitoring Instrument during NASA's Tropical Composition, Cloud and Climate Coupling Experiment (TC⁴), *Journal of Geophysical Research*, 115, 793, <https://doi.org/10.1029/2009JD013118>, 2010.
- Bucsela, E. J., Pickering, K. E., Allen, D. J., Holzworth, R., and Krotkov, N. A.: Midlatitude lightning NO_x production efficiency inferred from OMI and WWLLN data, *Journal of Geophysical Research: Atmospheres*, <https://doi.org/10.1029/2019JD030561>, 2019.
- Clark, S. K., Ward, D. S., and Mahowald, N. M.: Parameterization-based uncertainty in future lightning flash density, *Geophysical Research Letters*, 44, 2893–2901, <https://doi.org/10.1002/2017GL073017>, 2017.
- Finney, D. L., Doherty, R. M., Wild, O., Stevenson, D. S., MacKenzie, I. A., and Blyth, A. M.: A projected decrease in lightning under climate change, *Nature Climate Change*, 8, 210–213, <https://doi.org/10.1038/s41558-018-0072-6>, 2018.
- Krause, A., Kloster, S., Wilkenskeld, S., and Paeth, H.: The sensitivity of global wildfires to simulated past, present, and future lightning frequency, *Journal of Geophysical Research: Biogeosciences*, 119, 312–322, <https://doi.org/10.1002/2013JG002502>, 2014.
- Lapierre, J. L., Laughner, J. L., Geddes, J. A., Koshak, W., Cohen, R. C., and Pusede, S. E.: Observing U.S. regional variability in lightning NO₂ production rates, *Journal of Geophysical Research: Atmospheres*, <https://doi.org/10.1029/2019JD031362>, 2020.
- Pickering, K. E., Bucsela, E., Allen, D., Ring, A., Holzworth, R., and Krotkov, N.: Estimates of lightning NO_x production based on OMI NO₂ observations over the Gulf of Mexico, *Journal of Geophysical Research: Atmospheres*, 121, 8668–8691, <https://doi.org/10.1002/2015JD024179>, 2016.
- Romps, D. M.: Evaluating the future of lightning in cloud-resolving models, *Geophysical Research Letters*, <https://doi.org/10.1029/2019GL085748>, 2019.

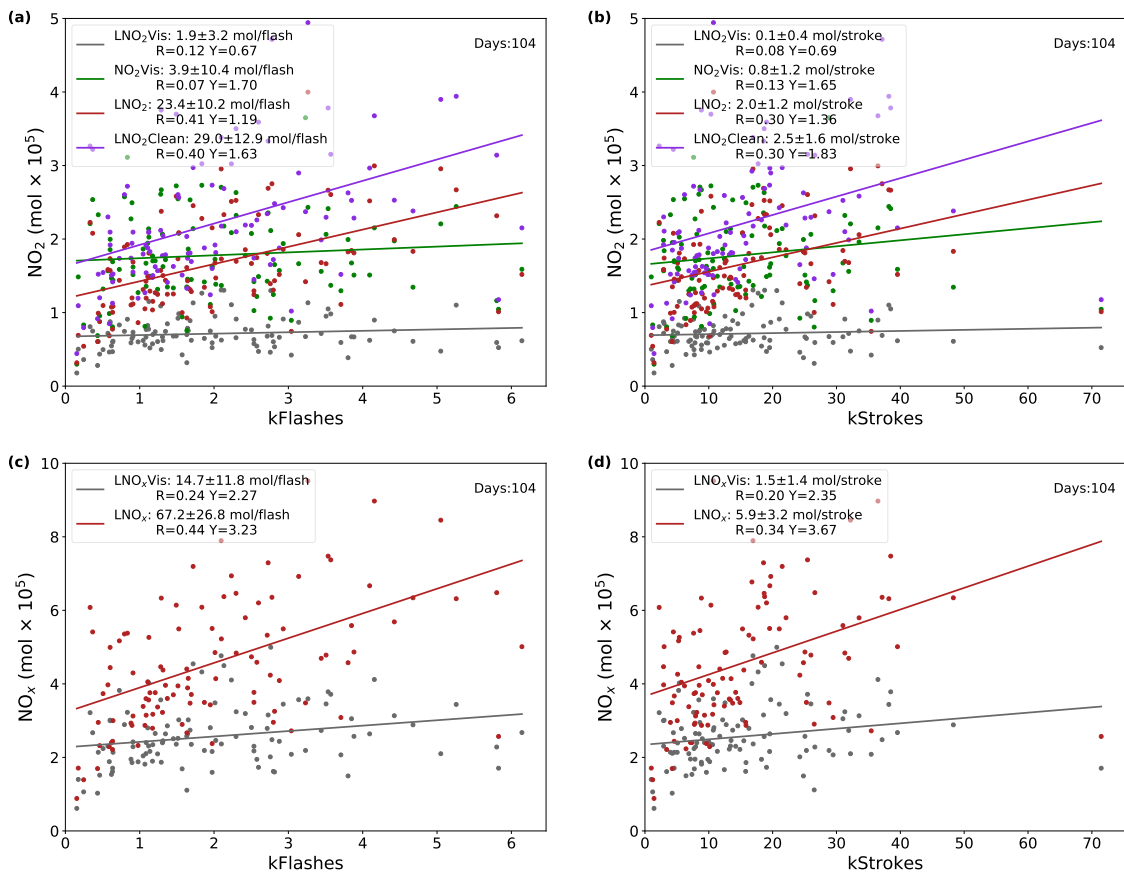


Figure R1 . Linear regression with CRF $\geq 90\%$ and a flash threshold of 1 flash box^{-1} or $3.4 \text{ strokes box}^{-1}$ per 2.4 h. (a) Daily NO₂Vis, LNO₂Vis, LNO₂ and LNO₂Clean versus ENTLN total flashes data. (b) Same as (a) but for strokes. (c) Daily LNO_xVis and LNO_x versus total flashes. (d) Same as (c) but for strokes.

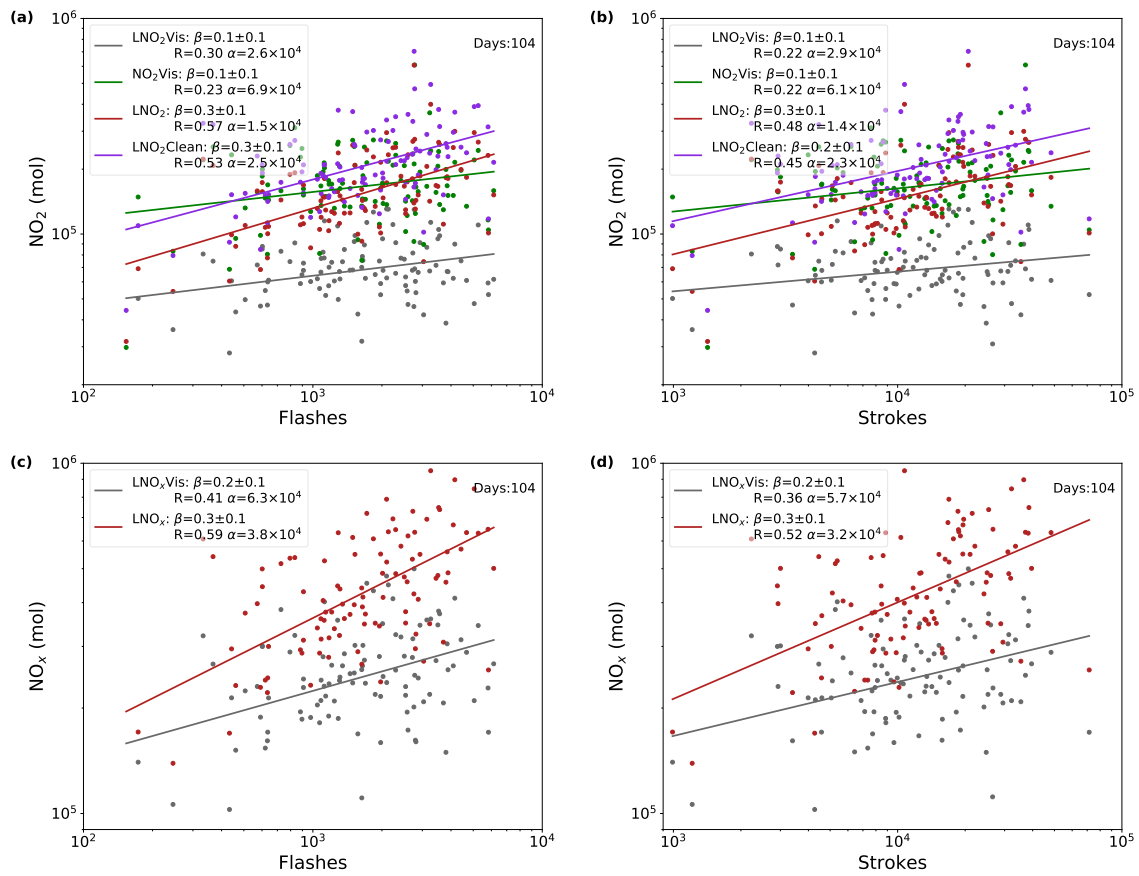


Figure R2 . Same as Fig. B1 but using log-log axes.

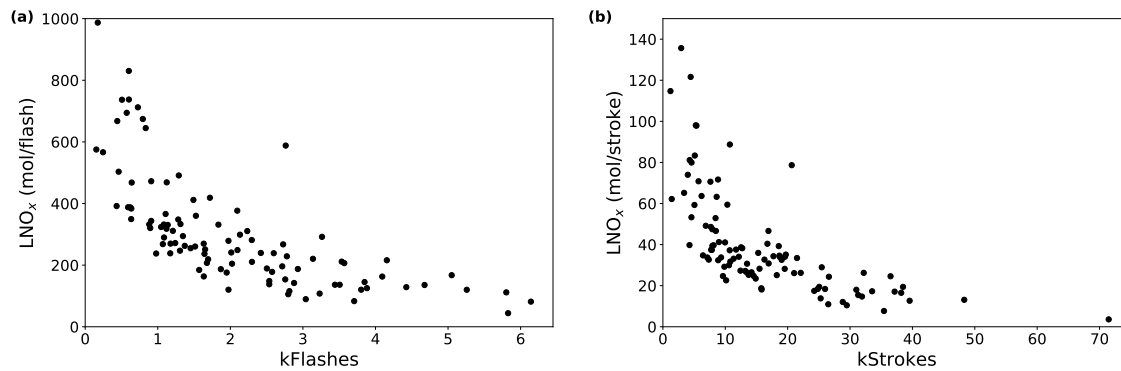


Figure R3 . (a) Daily LNO_x production efficiencies versus ENTLN total flashes data, with CRF $\geq 90\%$ and a flash threshold of 1 flash box⁻¹. (b) Same as (a) but for strokes.

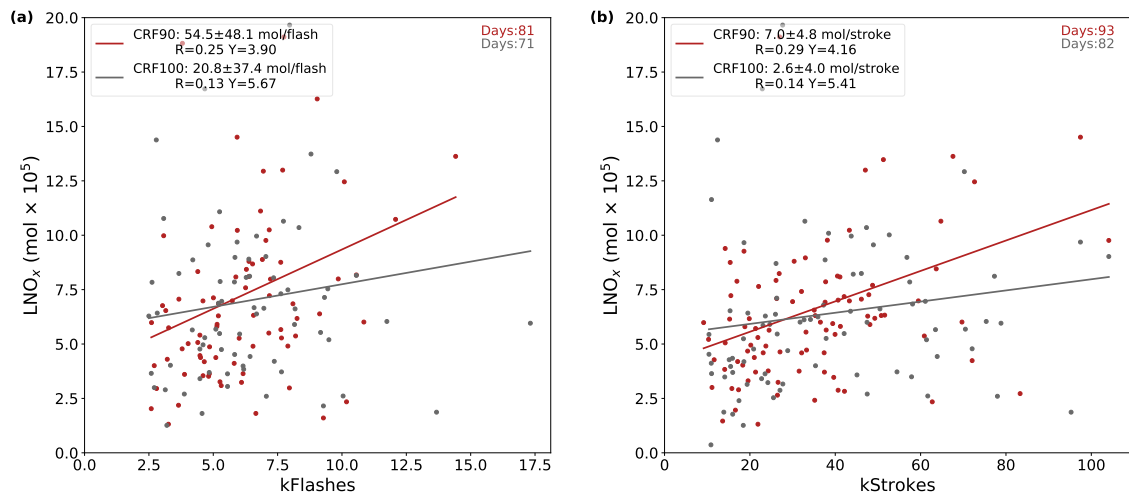


Figure R4 . (a) Daily LNO_x versus ENTLN total flashes data with CRF $\geq 90\%$ and CRF = 100%. (b) Same as (a) but for strokes.

Estimates of Lightning NO_x Production based on High Resolution OMI NO₂ Retrievals over the Continental US

Response to Anonymous Referee #2

Xin Zhang, Yan Yin, Ronald van der A, Jeff L. Lapierre, Qian Chen,
Xiang Kuang, Shuqi Yan, Jinghua Chen, Chuan He and Rulin Shi

March 8, 2020

We thank the reviewer for his/her positive comments and very careful reading of the main article. The individual corrections suggested are addressed below. The reviewer's comments will be shown in **red**, our response in **blue**, and changes made to the paper are shown in **black** block quotes. Unless otherwise indicated, page and line numbers correspond to the original paper. Figures, tables, or equations referenced as "Rn" are numbered within this response; if these are used in the changes to the paper, they will be replaced with the proper number in the final paper.

1) In the response to Referee #1:

Items 3 and 7:

Pickering et al. (2016) did subtract a tropospheric background. It was not done as part of the algorithm, but it was done as a final adjustment to the PE. In Section 6 of the Pickering et al. (2016) paper, 18% was subtracted from the derived PE value of 97 mol/flash which led to 80 mol/flash as the final value. The 18% was the mean of the two estimates of background derived from aircraft flights in the Gulf of Mexico region (3% and 33%). It needs to be made clear in the manuscript that Pickering et al. (2016) did not ignore the influence of background NO_x.

Thanks. We have corrected these according to your advice.

Since they considered NO₂ above the cloud as LNO₂ in the algorithm due to the difficulty and uncertainty in determining the background NO₂, their AMF and derived VCD of LNO_x (LNO₂) is named as AMF_{LNO_xClean} (AMF_{LNO₂Clean}) and LNO_xClean (LNO₂Clean), respectively. **Note that Pickering et al. (2016) considered the two estimates of background derived from aircraft flights in the Gulf of Mexico region (3% and 33%) and subtracted the mean value (18%) from the estimated mean LNO_x production efficiency (PE) for the background bias. However, we use the original algorithm directly without correction to distinguish the effect of different AMFs on LNO_x estimation in the remainder of this paper.**

2) In the response to Referee #1:

Item 4: The revision still sounds like (3% to >30%) is a range of uncertainty. The authors should say that this is the range of estimated background amounts.

Thank you for your remind. We have fixed it and merged it with the method of Pickering et al. (2016) (See No. 1).

3) Response to Referee #2:

Item 14:

The WRF-Chem level of neutral buoyancy parameterization stems from Price and Rind, but the details are based on Wong et al. (2013) Geosci. Model Dev., 6, 429–443, 2013 www.geosci-model-dev.net/6/429/2013/ doi:10.5194/gmd-6-429-2013. Please add the Wong et al. reference.

Thanks, added.

In addition, lightning flash rate based on the level of neutral buoyancy parameterization (**Price and Rind, 1992; Wong et al., 2013**) and LNO_x parameterizations are activated (200 mol NO flash⁻¹, the factor to adjust the predicted number of flashes is set to 1; hereinafter referred to as "1×200 mol NO flash⁻¹").

References

- Pickering, K. E., Bucsela, E., Allen, D., Ring, A., Holzworth, R., and Krotkov, N.: Estimates of lightning NO_x production based on OMI NO₂ observations over the Gulf of Mexico, *Journal of Geophysical Research: Atmospheres*, 121, 8668–8691, <https://doi.org/10.1002/2015JD024179>, 2016.
- Price, C. and Rind, D.: A simple lightning parameterization for calculating global lightning distributions, *Journal of Geophysical Research*, 97, 9919–9933, <https://doi.org/10.1029/92JD00719>, 1992.
- Wong, J., Barth, M. C., and Noone, D.: Evaluating a lightning parameterization based on cloud-top height for mesoscale numerical model simulations, *Geoscientific Model Development*, 6, 429–443, <https://doi.org/10.5194/gmd-6-429-2013>, 2013.

Estimates of Lightning NO_x Production based on High Resolution OMI NO_2 Retrievals over the Continental US

Response to Anonymous Referee #3

Xin Zhang, Yan Yin, Ronald van der A, Jeff L. Lapierre, Qian Chen,
Xiang Kuang, Shuqi Yan, Jinghua Chen, Chuan He and Rulin Shi

March 8, 2020

We thank the reviewer for his/her positive comments and very careful reading of the main article. The individual corrections suggested are addressed below. The reviewer's comments will be shown in **red**, our response in **blue**, and changes made to the paper are shown in **black** block quotes. Unless otherwise indicated, page and line numbers correspond to the original paper. Figures, tables, or equations referenced as " R_n " are numbered within this response; if these are used in the changes to the paper, they will be replaced with the proper number in the final paper.

1) Concerning the uncertainty of CP, there is one remaining issue. The study by Beirle et al. 2009 is based on model data. I don't think that it provides the uncertainty caused by CP which is needed for estimating the total uncertainty of the current study.

Instead, please check the uncertainty of the satellite CP retrieval given in the respective algorithm description, or in the input data, in order to do a modification of CP (analogue to the modification of Cloud Radiance Fraction) and derive the uncertainty from this modification.

Thanks for the suggestion. We have recalculated the uncertainty of CP based on Acarreta et al. (2004) and updated the related contents.

The cloud pressure bias is given as a function of cloud pressure and fraction by Acarreta et al. (2004) implying an uncertainty of 32% for LNO_2 and 34% for LNO_x .

Table R1 . Uncertainties for the estimation of LNO₂/flash, LNO_x/flash, LNO₂/stroke and LNO_x/stroke.

Type	Perturbation	LNO ₂ /flash ⁵	LNO _x /flash ⁵	LNO ₂ /stroke ⁵	LNO _x /stroke ⁵
BEHR tropopause pressure ¹	NASA product tropopause	6	4	6	4
Cloud radiance fraction ¹	± 5%	2	2	2	2
Cloud pressure ²	Variable	32	34	32	34
Surface pressure ¹	± 1.5%	0	0	0	0
Surface reflectivity ¹	± 17%	0	0	0	0
LNO ₂ profile ¹	2×500 mol NO flash ⁻¹	13	25	13	25
Profile location ¹	Quasi-Monte Carlo	0	1	0	1
Lightning detection efficiency ³	IC: ± 16%, CG: ± 5%	15	15	15	15
t _{window} ³	2 – 4 hours	10	10	8	8
LNO _x lifetime ³	2 – 12 hours	24	24	24	24
V _{strat} ⁴	-	10	10	10	10
Systematic errors in slant column ⁴	-	5	5	5	5
Tropospheric background ⁴	-	10	10	10	10
NO/NO ₂ ⁴	20% ± 15%	0	15	0	15
Net	-	49	56	48	56

PE_{uncertainty} = (Error_{rising perturbed value} - Error_{lowering perturbed value})/2 where Error_{perturbed value} = (PE_{perturbed value} - PE_{original value})/PE_{original value}.

¹Laughner et al. (2019) ²Acarreta et al. (2004) ³Lapierre et al. (2020) ⁴Allen et al. (2019) and Bucsele et al. (2019) ⁵Uncertainty (%)

References

- Acarreta, J. R., de Haan, J. F., and Stammes, P.: Cloud pressure retrieval using the O₂-O₂ absorption band at 477 nm, *Journal of Geophysical Research*, 109, 2165, <https://doi.org/10.1029/2003JD003915>, 2004.
- Allen, D. J., Pickering, K. E., Bucsela, E. J., Krotkov, N., and Holzworth, R.: Lightning NO_x Production in the Tropics as Determined Using OMI NO₂ Retrievals and WWLLN Stroke Data, *Journal of Geophysical Research: Atmospheres*, <https://doi.org/10.1029/2018JD029824>, 2019.
- Bucsela, E. J., Pickering, K. E., Allen, D. J., Holzworth, R., and Krotkov, N. A.: Midlatitude lightning NO_x production efficiency inferred from OMI and WWLLN data, *Journal of Geophysical Research: Atmospheres*, <https://doi.org/10.1029/2019JD030561>, 2019.
- Lapierre, J. L., Laughner, J. L., Geddes, J. A., Koshak, W., Cohen, R. C., and Pusede, S. E.: Observing U.S. regional variability in lightning NO₂ production rates, *Journal of Geophysical Research: Atmospheres*, <https://doi.org/10.1029/2019JD031362>, 2020.
- Laughner, J. L., Zhu, Q., and Cohen, R. C.: Evaluation of version 3.0B of the BEHR OMI NO₂ product, *Atmospheric Measurement Techniques*, 12, 129–146, <https://doi.org/10.5194/amt-12-129-2019>, 2019.

Estimates of Lightning NO_x Production based on High Resolution OMI NO₂ Retrievals over the Continental US

Xin Zhang^{1,2}, Yan Yin^{1,2}, Ronald van der A^{2,3}, Jeff L. Lapierre⁴, Qian Chen^{1,2}, Xiang Kuang^{1,2}, Shuqi Yan², Jinghua Chen^{1,2}, Chuan He^{1,2}, and Rulin Shi^{1,2}

¹ Collaborative Innovation Center on Forecast and Evaluation of Meteorological Disasters/Key Laboratory for Aerosol-Cloud-Precipitation of China Meteorological Administration, Nanjing University of Information Science and Technology (NUIST), Nanjing 210044, China

² Department of Atmospheric Physics, Nanjing University of Information Science and Technology (NUIST), Nanjing 210044, China

³ Royal Netherlands Meteorological Institute (KNMI), Department of Satellite Observations, De Bilt, the Netherlands

⁴ Earth Networks, Germantown, Maryland, USA

Correspondence: Yan Yin (yinyan@nuist.edu.cn)

Abstract. Lightning serves as the dominant source of nitrogen oxides (NO_x = NO + NO₂) in the upper troposphere (UT), with strong impact on ozone chemistry and the hydroxyl radical production. However, the production efficiency (PE) of lightning nitrogen oxides (LNO_x) is still quite uncertain (32 – 1100 mol NO per flash). Satellite measurements are a powerful tool to estimate LNO_x directly as compared to conventional platforms. To apply satellite data in both clean and polluted regions, a new algorithm for calculating LNO_x has been developed that uses the Berkeley High Resolution (BEHR) v3.0B NO₂ **product retrieval algorithm** and the Weather Research and Forecasting-Chemistry (WRF-Chem) model. LNO_x PE over the continental US is estimated using the NO₂ product of the Ozone Monitoring Instrument (OMI) **satellite data** and the Earth Networks Total Lightning Network (ENTLN) data. Focusing on the summer season during 2014, we find that the lightning NO₂ (LNO₂) PE is 32 ± 15 mol NO₂ flash⁻¹ and 6 ± 3 mol NO₂ stroke⁻¹ while LNO_x PE is $90 \pm 49-50$ mol NO_x flash⁻¹ and $17 \pm 9-10$ mol NO_x stroke⁻¹. Results reveal that our method reduces **the** sensitivity to the background NO₂ and includes much of the below-cloud LNO₂. As the LNO_x parameterization varies in studies, the sensitivity of our calculations to the setting of the amount of lightning NO (LNO) is evaluated. Careful consideration of the ratio of LNO₂ to NO₂ is also needed, given its large influence on the estimation of LNO₂ PE.

1 Introduction

Nitrogen oxides (NO_x) near the Earth's surface are mainly produced by soil, biomass burning and fossil fuel combustion, while NO_x in the middle and upper troposphere originates largely from lightning and aircraft emissions. NO_x plays an important role in the production of ozone (O₃) and the hydroxyl radical (OH). While the anthropogenic sources of NO_x are largely known, lightning nitrogen oxides (LNO_x) are still the source with the greatest uncertainty, though they are estimated to range between 2 and 8 Tg N yr⁻¹ (Schumann and Huntrieser, 2007). LNO_x is produced in the upper troposphere (UT) by O₂ and N₂ dissociation in the hot lightning channel as described by the Zel'dovich mechanism (Zel'dovich and Raizer, 1967). With the recent updates

of UT NO_x chemistry, the day time lifetime of UT NO_x is evaluated to be ~ 3 h near thunderstorms and ~ 0.5 – 1.5 days away from thunderstorms (Nault et al., 2016, 2017). This results in enhanced O₃ production in the cloud outflow of active convection (Pickering et al., 1996; Hauglustaine et al., 2001; DeCaria et al., 2005; Ott et al., 2007; Dobber et al., 2008; Allen et al., 2010; Finney et al., 2016). As O₃ is known as a greenhouse gas, strong oxidant and absorber of ultraviolet radiation (Myhre et al., 2013), the contributions of LNO_x to O₃ production also have an effect on climate forcing. Finney et al. (2018) found different impacts on atmospheric composition and radiative forcing when simulating future lightning using a new upward cloud ice flux (IFLUX) method versus the commonly used cloud-top height (CTH) approach. While global lightning is predicted to increase by 5 — 16% over the next century with the CTH approach (Clark et al., 2017; Banerjee et al., 2014; Krause et al., 2014), a 15% decrease in global lightning was estimated with IFLUX in 2100 under a strong global warming scenario (Finney et al., 2018). As a result of the different effects on radiative forcing from ozone and methane, a net positive radiative forcing was found with the CTH approach while there is little net radiative forcing with the IFLUX approach (Finney et al., 2018). However, the convective available potential energy (CAPE) times the precipitation rate (P) proxy predicts a 12 ± 5% increase in the Continental US (CONUS) lightning strike rate per kelvin of global warming (Romps et al., 2014), while the IFLUX proxy predicts the lightning will only increase 3.4%/K over the CONUS. Recently, Romps (2019) compared the CAPE × P proxy and IFLUX method in cloud-resolving models. They ~~report~~reported that higher CAPE and updraft velocities caused by global warming could lead to the large increases in tropical lightning simulated by CAPE × P proxy, while IFLUX proxy predicts little change in tropical lightning because of the small changes in ~~water mass fluxes~~the mass flux of ice.

In the view of the ~~region~~regionally dependent lifetime of NO_x and the difficulty of measuring LNO_x directly, a better understanding of the LNO_x production is required, especially in the tropical and mid-latitude regions in summer. Using its distinct spectral absorption lines in the near-ultraviolet (UV) and visible (VIS) range (Platt and Perner, 1983), NO₂ can be measured by satellite instruments like the Global Ozone Monitoring Experiment (GOME; Burrows et al., 1999; Richter et al., 2005), Scanning Imaging Absorption Spectrometer for Atmospheric Chartography (SCIAMACHY; Bovensmann et al., 1999), the Second Global Ozone Monitoring Experiment (GOME-2; Callies et al., 2000) and the Ozone Monitoring Instrument (OMI; Levelt et al., 2006). OMI has the highest spatial resolution, least instrument degradation and longest record among these satellites (Krotkov et al., 2017). Satellite measurements of NO₂ are a powerful tool compared to conventional platforms, because of its global coverage, constant instrument features and temporal continuity.

Recent studies have determined and quantified LNO_x using satellite observations. Beirle et al. (2004) constrained the LNO_x production to 2.8 (0.8 – 14) Tg N yr⁻¹ by combining GOME NO₂ data and flash counts from the Lightning Imaging Sensor (LIS) aboard the Tropical Rainfall Measurement Mission (TRMM) over Australia. Boersma et al. (2005) estimated the global LNO_x production of 1.1 – 6.4 Tg N yr⁻¹ by comparing GOME NO₂ with distributions of LNO₂ modeled by Tracer Model 3 (TM3). Martin et al. (2007) analyzed SCIAMACHY NO₂ columns with Goddard Earth Observing System chemistry model (GEOS-Chem) simulations to identify LNO_x production amounting to 6 ± 2 Tg N yr⁻¹.

As these methods focus on monthly or ~~yearly~~annual mean NO₂ column densities, more recent studies applied specific approaches to investigate LNO_x directly over active convection. Beirle et al. (2006) estimated LNO_x as 1.7 (0.6 – 4.7) Tg N yr⁻¹ based on a convective system over the Gulf of Mexico, using National Lightning Detection Network (NLDN) observations

and GOME NO₂ column densities. However, ~~this study it is~~ assumed that all the enhanced NO₂ originated from lightning and did not consider the contribution of anthropogenic emissions. Beirle et al. (2010) analyzed LNO_x production systematically using the global dataset of SCIAMACHY NO₂ observations combined with flash data from the World Wide Lightning Location Network (WWLLN). Their analysis was restricted to 30×60 km² satellite pixels where the flash rate exceeded 1 flash km⁻² 60 hr⁻¹. But they found LNO_x production to be highly variable and correlations between flash rate densities and LNO_x production ~~are were~~ low in some cases. Bucselá et al. (2010) ~~estimate estimated~~ LNO_x production as ~ 100 – 250 mol NO_x/flash for four cases, using the DC-8 and OMI data during NASA's Tropical Composition, Cloud and Climate Coupling Experiment (TC⁴).

Based on the approach used by Bucselá et al. (2010), a special algorithm was developed by Pickering et al. (2016) to retrieve LNO_x from OMI and the WWLLN. The algorithm takes the OMI tropospheric slant column density (SCD) of NO₂ (S_{NO₂}) as 65 the tropospheric slant column density of LNO₂ (S_{LNO₂}) by using cloud radiance fraction (CRF) greater than 0.9 to minimize or screen the lower tropospheric background. To convert the S_{LNO₂} to the tropospheric vertical column density (VCD) of LNO_x (V_{LNO_x}), an air mass factor (AMF) is calculated by dividing the a priori S_{LNO₂} by the a priori V_{LNO_x}. ~~Since they considered NO₂ above the cloud as LNO₂ in the algorithm due to the difficulty and uncertainty in determining the background NO₂, their AMF and derived VCD of LNO_x (LNO₂) is named as AMF_{LNO_xClean} (AMF_{LNO₂Clean}) and LNO_xClean (LNO₂Clean), respectively. Unless otherwise specified, abbreviations S and V are respectively defined as the tropospheric SCD and VCD in this paper.~~ 70 Since they considered NO₂ above the cloud as LNO₂ in the algorithm due to the difficulty and uncertainty in determining the background NO₂, their AMF and derived VCD of LNO_x (LNO₂) is named as AMF_{LNO_xClean} (AMF_{LNO₂Clean}) and LNO_xClean (LNO₂Clean), respectively. Note that Pickering et al. (2016) considered the two estimates of background derived from aircraft flights in the Gulf of Mexico region (3% ~>30%) in this region (Pickering et al., 2016) and 33% and subtracted the mean value (18%) from the estimated mean LNO_x production efficiency (PE) for the background bias. However, we use the original algorithm directly without 75 correction to distinguish the effect of different AMFs on LNO_x estimation in the remainder of this paper. Unless otherwise specified, abbreviations S and V are respectively defined as the tropospheric SCD and VCD in this paper. 80

More recently Bucselá et al. (2019) obtained an average ~~production efficiency (PE) PE~~ of 180 ± 100 mol ~~per NO_x/flash~~ over East Asia, Europe and North America based on a modification of the method used in Pickering et al. (2016). A power function between LNO_x and lightning flash rate was established, while the minimum flash-rate threshold was not applied. The 85 tropospheric NO_x background was removed by subtracting the temporal average of NO_x at each box where the value was weighted by the number of OMI pixels which meet the optical cloud pressure and CRF criteria required to be considered deep convection but ~~has have~~ 1 flash or less instead. The lofted pollution was considered as 15% of total NO_x according to the estimation from DeCaria et al. (2000, 2005) and the average chemical delay was adjusted by 15% following the 3-hour LNO_x lifetime in the nearby field of convection (Nault et al., 2017). However, there were negative LNO_x values caused by the 90 overestimation of the tropospheric background and stratospheric NO₂ at some locations.

On the other hand, [Lapierre et al. \(2019\)](#)-[Lapierre et al. \(2020\)](#) constrained LNO_2 to $1.1 \pm 0.6-0.2$ mol NO_2 /stroke for intracloud (IC) strokes and $10.0-10.7 \pm 4.9-2.5$ mol NO_2 /stroke for cloud-to-ground (CG) strokes over the CONUS. LNO_2 per stroke was scaled to $54.4-24.2$ mol NO_x /flash using mean values of strokes per flash and the ratio of NO_x to NO_2 in the UT. They used the regridded Berkeley High-Resolution (BEHR) V3.0A $0.05^\circ \times 0.05^\circ$ "visible only" NO_2 VCD (V_{vis}) product which includes two parts of NO_2 that can be "seen" by the satellite. The first part is the NO_2 above clouds (pixels with CRF > 0.9) and the second part is the NO_2 detected from cloud free areas. A threshold of 3×10^{15} molecules cm^{-2} , the typical urban NO_2 concentration, was applied to mask the contaminated grid cells (Beirle et al., 2010; Laughner and Cohen, 2017). The main difference between [Lapierre et al. \(2019\)](#)-[Lapierre et al. \(2020\)](#) and Pickering et al. (2016) is the air mass factor for lightning (AMF_{LNO_x}) implemented in the basic algorithm. In [Lapierre et al. \(2019\)](#)-[Lapierre et al. \(2020\)](#), the air mass factor was used to convert S_{NO_2} to V_{vis} , while in Pickering et al. (2016) it was used to convert S_{LNO_2} to V_{LNO_x} , assuming that all S_{NO_2} is generated by lightning.

To apply the approach used by Bucselo et al. (2010), Pickering et al. (2016), Bucselo et al. (2019) and [Lapierre et al. \(2019\)](#)-[Lapierre et al. \(2020\)](#) without geographic restrictions, the contamination by anthropogenic emissions must be taken into account in detail. The Weather Research and Forecasting (WRF) model coupled with chemistry (WRF-Chem) has been employed to evaluate the convective transport and chemistry in many studies (Barth et al., 2012; Wong et al., 2013; Fried et al., 2016; Li et al., 2017). Meanwhile, Laughner and Cohen (2017) showed that the OMI AMF is increased by $\sim 35\%$ for summertime when LNO_2 simulated by WRF-Chem is included in the a priori profiles to match aircraft observations. The simulation agrees with observed NO_2 profiles and the bias of AMF related to these observations is reduced to $< \pm 4\%$ for OMI viewing geometries.

In this paper, we focus on the estimation of LNO_2 production per flash (LNO_2 /flash), LNO_x production per flash (LNO_x /flash), LNO_2 production per stroke (LNO_2 /stroke) and LNO_x production per stroke (LNO_x /stroke) in May–August (MJJA) 2014 by developing an algorithm similar to Pickering et al. (2016) based on the BEHR NO_2 retrieval algorithm (Laughner et al., 2018a, b), but it performs better over background NO_2 sources. Section 2 describes the satellite data, lightning data, model settings and the algorithm in detail. Section 3 explores the suitable data criteria, compares different methods and evaluates the effect of background NO_2 , cloud and LNO_x parameterization on LNO_x production estimation. Section 4 examines the effect of different sources of the uncertainty on the results. Conclusions are summarized in Section 5.

2 Data and Methods

2.1 Ozone Monitoring Instrument (OMI)

OMI is carried on the Aura satellite (launched in 2004), a member of A-train satellite group (Levelt et al., 2006, 2018). OMI passes over the equator at $\sim 13:45$ LT (ascending node) and has a swath width of 2600 km, with a nadir field-of-view resolution of 13×24 km². Since the beginning of 2007, some of the measurements have become useless as a result of anomalous radiances called the "row anomaly" (Dobber et al., 2008; KNMI, 2012). For the current study, we used the NASA standard product V3.0 (Krotkov et al., 2017) as input to the LNO_x retrieval algorithm.

The main steps of calculating the NO_2 tropospheric VCD (V_{NO_2}) in the NASA product include:

1. SCDs are determined by the OMI-optimized differential optical absorption spectroscopy (DOAS) spectral fit;
 - 125 2. A corrected ("de-stripped") SCD is obtained by subtracting the cross-track bias caused by an instrument artifact from the measured slant column;
 3. The AMF for stratospheric (AMF_{strat}) or tropospheric column (AMF_{trop}) is calculated from the NO_2 ~~profile~~ profiles integrated vertically using weighted scattering weights with the a priori profiles. These profiles are obtained from GMI monthly mean profiles using four years (2004 – 2007) simulation;
 - 130 4. The stratospheric NO_2 VCD (V_{strat}) is calculated from the subtraction of a priori contribution from tropospheric NO_2 and a three-step (interpolation, filtering, and smoothing) algorithm (Bucsela et al., 2013);
 5. V_{strat} is converted to the slant column using AMF_{strat} and subtracted from the measured SCDs to yield S_{NO_2} , leading to $V_{NO_2} = S_{NO_2}/AMF_{trop}$.
- Based on this method, we developed a new AMF_{LNO_x} to obtain the desired V_{LNO_x} ($V_{LNO_x} = S_{NO_2}/AMF_{LNO_x}$) ~~to-replace-by~~
135 replacing the original step 5. Details of this algorithm are discussed in section 2.4.

2.2 The Earth Networks Total Lightning Detection Network (ENTLN)

The Earth Networks Total Lightning Network (ENTLN) operates a system of over 1500 ground-based stations around the world with more than 900 sensors installed in the CONUS (Zhu et al., 2017). Both IC and CG lightning flashes are located by the sensors with detection frequency ranging from 1 Hz to 12 MHz based on the electric field pulse polarity and wave shapes.
140 Groups of pulses are classified as a flash if they are within 700 ms and 10 km. In the preprocessed data obtained from the ENTLN, both strokes and lightning flashes composed of one or more strokes are included.

Rudlosky (2015) compared ENTLN combined events (IC and CG) with LIS flashes and found that the relative flash detection efficiency of ENTLN over CONUS increases from 62.4% during 2011 to 79.7% during 2013. ~~Lapierre et al. (2019)~~
Lapierre et al. (2020) also compared combined ENTLN and the NLDN dataset with data from the LIS during 2014 and found
145 the detection efficiencies of IC flashes and strokes to be 88% and 45%, respectively. Since we only use the ENTLN data in 2014 as ~~Lapierre et al. (2019)~~ Lapierre et al. (2020) and NLDN detection efficiency of IC pulses should be lower than 33% which is calculated by the data in 2016 (Zhu et al., 2016), only the IC flashes and strokes are divided by 0.88 and 0.45, respectively, while CG flashes and strokes are unchanged because of the high detection efficiency.

2.3 Model Description

150 The present study uses WRF-Chem version 3.5.1 (Grell et al., 2005) with a horizontal grid size of $12 \times 12 \text{ km}^2$ and 29 vertical levels (Fig. 1). The initial and boundary conditions of meteorological parameters are provided by the North American Regional Reanalysis (NARR) dataset with a 3 hourly time resolution. Based on Laughner et al. (2018b), 3D wind fields, temperature and water vapor are nudged towards the NARR data. Outputs from the version 4 of Model for Ozone and Related chemical Tracers (MOZART-4; Emmons et al., 2010) ~~were-are~~
155 Anthropogenic emissions are driven by the 2011 National Emissions Inventory (NEI), scaled to model years by the Environmental Protection Agency annual total emissions (EPA and OAR, 2015). The Model of Emissions of Gases and Aerosol from

Nature (MEGAN; Guenther et al., 2006) is used for biogenic emissions. The chemical mechanism is the version 2 of Regional Atmospheric Chemistry Mechanism (RACM2; Goliff et al., 2013) with updates from Browne et al. (2014) and Schwantes et al. (2015). In addition, lightning flash rate based on the level of neutral buoyancy parameterization (~~Price and Rind, 1992~~) (Price and Rind, 1992; Wong et al., 2013) and LNO_x parameterizations are activated (200 mol NO flash⁻¹, the factor to adjust the predicted number of flashes is set to 1; hereinafter referred to as "1×200 mol NO flash⁻¹"). ~~Although the simulated Simulated~~ total flash densities are higher ~~in than~~ ENTLN observations over the Southeast US and lower ~~than observations~~ in the North Central US (Fig. 2), ~~the criteria in Sect. 3.1 could limit this effect on the estimation of~~. ~~The impact of these biases on LNO_x production and Sect. is discussed and mitigated in Sect. 3.1 and 3.4 will use another simulation to test this problem~~. The bimodal profile modified from the standard Ott et al. (2010) profile (Laughner and Cohen, 2017) is employed as the vertical distribution of lightning NO (LNO) in WRF-Chem, while outputs of LNO and LNO₂ profiles are defined as the difference of vertical profiles between simulations with and without lightning.

2.4 Method for Deriving AMF

The V_{LNO_x} near convection is calculated according:

$$170 \quad V_{LNO_x} = \frac{S_{NO_2}}{AMF_{LNO_x}} \quad (1)$$

where S_{NO_2} is the OMI-measured tropospheric slant column NO₂ and AMF_{LNO_x} is a customized lightning air mass factor. The concept of AMF_{LNO_x} was also used in Beirle et al. (2009) to investigate the sensitivity of satellite instruments ~~for to~~ freshly produced lightning NO_x. In order to estimate LNO_x, we define the AMF_{LNO_x} as the ratio of the "visible" modeled NO₂ slant column to the total modeled tropospheric LNO_x vertical column (derived from the a priori NO and NO₂ profiles, scattering weights, and ~~radiance cloud cloud~~ radiance fraction):

$$175 \quad AMF_{LNO_x} = \frac{(1 - f_r) \int_{p_{surf}}^{p_{tp}} w_{clear}(p) NO_2(p) dp + f_r \int_{p_{cloud}}^{p_{tp}} w_{cloudy}(p) NO_2(p) dp}{\int_{p_{surf}}^{p_{tp}} LNO_x(p) dp} \quad (2)$$

where f_r is the ~~radiance cloud fraction~~ cloud radiance fraction (CRF), p_{surf} is the surface pressure, p_{tp} is the tropopause pressure, p_{cloud} is the cloud optical pressure (CP), w_{clear} and w_{cloudy} are respectively the pressure dependent scattering weights from the TOMRAD lookup table (Bucsela et al., 2013) for clear and cloudy parts, and $NO_2(p)$ is the modeled NO₂ vertical profile. Details of these standard parameters and calculation methods are given in Laughner et al. (2018a). $LNO_x(p)$ is the LNO_x vertical profile calculated by the difference of vertical profiles between WRF-Chem simulations with and without lightning.

Please note that the CP is a reflectance-weighted pressure retrieved by the collision-induced O₂-O₂ absorption band near 477 nm (Acarreta et al., 2004; Sneepe et al., 2008; Stammes et al., 2008). For a deep convective cloud with lightning, the CP lies below the geometrical cloud top which is much closer to that detected by thermal infrared sensors, such as the CloudSat and the Aqua MODerate-resolution Imaging Spectrometer (MODIS) (Vasilkov et al., 2008; Joiner et al., 2012). Hence, much of the tropospheric NO₂ measured by OMI lies inside the cloud rather than above the cloud top. In the following, "above cloud" or "below cloud" is relative to the cloud pressure detected by OMI. The sensitivity study of Beirle et al. (2009) compared the

chemical ~~compositions~~ composition from the cloud bottom to the cloud top and revealed that a significant fraction of the NO_2 within the cloud originating from lightning can be detected by the satellite. This valuable cloud pressure concept has been applied not only in the LNO_x research but also in the cloud slicing method of deriving the UT O_3 and NO_x (Ziemke et al., 2009; Choi et al., 2014; Strode et al., 2017; Ziemke et al., 2017; Marais et al., 2018). As discussed in Pickering et al. (2016), the ratio of V_{LNO_2} seen by OMI to V_{LNO_x} is partly influenced by p_{cloud} . The effects of LNO_2 below the cloud will be discussed in Sect. 3.4.

To compare our results with those of Pickering et al. (2016) and ~~Lapierre et al. (2019)~~ Lapierre et al. (2020), we calculate their $\text{AMF}_{\text{LNO}_x\text{Clean}}$ and $\text{AMF}_{\text{NO}_2\text{Vis}}$ respectively:

$$\text{AMF}_{\text{LNO}_x\text{Clean}} = \frac{(1 - f_r) \int_{p_{\text{surf}}}^{p_{\text{tp}}} w_{\text{clear}}(p) \text{LNO}_2(p) dp + f_r \int_{p_{\text{cloud}}}^{p_{\text{tp}}} w_{\text{cloudy}}(p) \text{LNO}_2(p) dp}{\int_{p_{\text{surf}}}^{p_{\text{tp}}} \text{LNO}_x(p) dp} \quad (3)$$

$$\text{AMF}_{\text{NO}_2\text{Vis}} = \frac{(1 - f_r) \int_{p_{\text{surf}}}^{p_{\text{tp}}} w_{\text{clear}}(p) \text{NO}_2(p) dp + f_r \int_{p_{\text{cloud}}}^{p_{\text{tp}}} w_{\text{cloudy}}(p) \text{NO}_2(p) dp}{(1 - f_g) \int_{p_{\text{surf}}}^{p_{\text{tp}}} \text{NO}_2(p) dp + f_g \int_{p_{\text{cloud}}}^{p_{\text{tp}}} \text{NO}_2(p) dp} \quad (4)$$

where f_g is the geometric cloud fraction and $\text{LNO}_2(p)$ is the modeled LNO_2 vertical profile. Besides these AMFs, another AMF called $\text{AMF}_{\text{LNO}_2\text{Vis}}$ is developed for ~~comparison-later~~ later comparison.

$$\text{AMF}_{\text{LNO}_2\text{Vis}} = \frac{(1 - f_r) \int_{p_{\text{surf}}}^{p_{\text{tp}}} w_{\text{clear}}(p) \text{NO}_2(p) dp + f_r \int_{p_{\text{cloud}}}^{p_{\text{tp}}} w_{\text{cloudy}}(p) \text{NO}_2(p) dp}{(1 - f_g) \int_{p_{\text{surf}}}^{p_{\text{tp}}} \text{LNO}_2(p) dp + f_g \int_{p_{\text{cloud}}}^{p_{\text{tp}}} \text{LNO}_2(p) dp} \quad (5)$$

A full ~~list of definitions of~~ definition list of the used AMFs is shown in Appendix A.

2.5 Procedures for Deriving LNO_x

V_{LNO_x} is re-gridded to $0.05^\circ \times 0.05^\circ$ grids using the constant value method (Kuhlmann et al., 2014). Then, it is analyzed in $1^\circ \times 1^\circ$ grid boxes with a minimum of fifty valid $0.05^\circ \times 0.05^\circ$ grids to minimize the noise. The ~~minimum value is between five satellite pixels in Pickering et al. (2016) and three satellite pixels in Bucsela et al. (2019) or Allen et al. (2019). The main procedures used to derive~~ main procedures of deriving LNO_x are as follows:

CRFs (~~CRFs~~ CRF $\geq 70\%$, ~~CRFs~~ CRF $\geq 90\%$ and ~~CRFs~~ CRF = 100%) and $\text{CP} \leq 650$ hPa are various criteria of deep convective clouds for OMI pixels (Ziemke et al., 2009; Choi et al., 2014; Pickering et al., 2016). The effect of different CRFs on the retrieved LNO_x is explored in section 3.2. Furthermore, another criterion of cloud ~~fractions~~ CFs fraction (CF) is applied to the WRF-Chem results for the successful simulation of convection. The ~~CFs are~~ CF is defined as the maximum cloud fraction calculated by the Xu-Randall method between 350 and 400 hPa (Xu and Randall, 1996; Strode et al., 2017). This atmospheric layer (between 350 and 400 hPa) avoids any biases in the simulation of high clouds. We choose ~~CFs~~ CF $\geq 40\%$ suggested by Strode et al. (2017) to determine cloudy or clear for each simulation grid.

Besides cloud properties, a time period and sufficient flashes (or strokes) are required for fresh LNO_x to be detected by OMI. The time window (t_{window}) is the hours prior to the OMI overpass time. t_{window} is limited to 2.4 h by the mean wind speed at pressure levels 500 – 100 hPa during OMI overpass time and the square root of the $1^\circ \times 1^\circ$ box over the CONUS

(Lapierre et al., 2019)(Lapierre et al., 2020). Meanwhile, 2400 flashes box^{-1} and 8160 strokes box^{-1} per 2.4 hour time window are chosen as sufficient for detecting LNO_x (Lapierre et al., 2019)(Lapierre et al., 2020). These criteria will result in a low bias in the PE results, as Bucselá et al. (2019) found that the PE is larger at small flash rates which are discarded here. Since our study focuses on developing a new AMF and compare results with other works using the similar lightning thresholds (Lapierre et al., 2020; Pickering et al., 2016), we will only discuss results based on the strict criteria in the main text. For comparisons between 2400 flashes box^{-1} criterion and 1 flash box^{-1} criterion, scatter diagrams using different lightning criteria are presented in Appendix B.

To ensure that lightning flashes are simulated successfully by WRF-Chem, the threshold of simulated total lightning flashes (TL) per box is set to 1000, which is fewer than that used by the ENTLN lightning observation, considering the uncertainty of lightning parameterization. In view of other NO_2 sources in addition to LNO_2 , the ratio of modeled lightning NO_2 above cloud (LNO_2Vis) to modeled NO_2 above cloud (NO_2Vis) is defined to check whether enough LNO_2 can be detected by OMI. The ratio $\geq 50\%$ indicates that more than half of the NO_x above the cloud must have a has an LNO_x source.

Finally, the NO_2 lifetime against oxidation should be taken into account. As estimated by Nault et al. (2016), the lifetime (τ) of NO_2 in the near field of convections is ~ 3 h. The initial value of NO_2 is solved by Eq. 6 as

$$NO_2(0) = NO_2(OMI) \times e^{0.5t/\tau} \quad (6)$$

where $NO_2(0)$ is the moles of NO_2 emitted at time $t = 0$, $NO_2(OMI)$ is the moles of NO_2 measured at the OMI overpass time and $0.5t$ is the half cross grid time which is 1.2 h, assuming that lightning occurred at the center of each $1^\circ \times 1^\circ$ box. For each grid box, the mean LNO_x vertical column is obtained by averaging V_{LNO_x} values from all regridded $0.05^\circ \times 0.05^\circ$ pixels in the box. This mean value is converted to moles LNO_x using the dimensions of the grid box. Two methods are applied to estimate the seasonal mean $\text{LNO}_2/\text{flash}$, $\text{LNO}_x/\text{flash}$, $\text{LNO}_2/\text{stroke}$ and $\text{LNO}_x/\text{stroke}$:

(1) summation method: dividing the sum of LNO_x by the sum of flashes (or strokes) in each $1^\circ \times 1^\circ$ box in MJJA 2014;

(2) linear regression method: applying the linear regression to daily mean values of LNO_x and flashes (or strokes).

240 3 Results

3.1 Criteria Determination

To determine the suitable criteria from conditions defined in section 2.5, six different combinations are defined (Table 1) and applied to the original data with a linear regression method (Table 2).

A daily search of the NO_2 product for coincident ENTLN flash (stroke) data results in 99 (102) valid days under the CRF90_ENTLN condition. Taking the ~~flashes-flash~~ type ENTLN data as an example, the number of valid days decreases from 99 to 81 under the CRF90_ENTLN_TL1000_ratio50 condition, while $\text{LNO}_x/\text{flash}$ increases from 52.1 ± 51.1 mol/flash to 54.5 ± 48.1 mol/flash. The result is almost the same as that under the CRF90_ENTLN_TL1000 condition which is without the condition of ~~ratio $\geq 50\%$ more than half of the above-cloud NO_x having an LNO_x source~~. Although this indicates the criterion of TL works well, it is better to include the ratio criterion in case of some exceptions in the different AMF methods.

250 Since $CF \geq 40\%$ leads to a sharp loss of valid numbers and production, therefore, it is not a suitable criterion. Instead the CRF criteria are used. Finally, coincident ENTLN data, $TL \geq 1000$ and $ratio \geq 50\%$ are chosen as the thresholds to explore the effects of three different CRF conditions ($CRF \geq 70\%$, $CRF \geq 90\%$ and $CRF = 100\%$) on LNO_x production (Table 3).

~~LNO_x production for different thresholds of CRF with coincident ENTLN data, $TL \geq 1000$ and $ratio \geq 50\%$. CRF (%) ENTLN data type¹ LNO_x /flash or LNO_x /stroke R-value Interecept (10^5 mol) Days² 70 Flash 35.7 ± 36.8 0.21 4.91 85 90 Flash 54.5 ± 48.1 0.25 3.90 81 100 Flash 20.8 ± 37.4 0.13 5.67 71 70 Stroke 4.1 ± 3.9 0.21 5.16 96 90 Stroke 7.0 ± 4.8 0.29 4.16 93 100 Stroke 2.6 ± 4.0 0.14 5.41 82~~

Apart from the fewer valid days under higher CRF conditions ($CRF \geq 90\%$ and $CRF = 100\%$), LNO_x /flash increases from 35.7 ± 36.8 mol/flash to 54.5 ± 48.1 mol/flash and decreases again to 20.8 ± 37.4 mol/flash while LNO_x /stroke enhances from 4.1 ± 3.9 mol/stroke to 7.0 ± 4.8 mol/stroke and drops again to 2.6 ± 4.0 mol/stroke (Table 3), as the CRF criterion increases from 70% to 90% and to 100%. When the CRF increases from 90% to 100%, the LNO_x PE decreases because of the higher lightning density with fewer LNO_x (not shown). The increment of LNO_x PE caused by the CRF increase from 70% to 90% is opposite to the result of Pickering et al. (2016). This is an effect of the consideration of NO_2 contamination transported from the boundary layer in our method. Although enhanced NO_x is often observed in regions with $CRF > 70\%$ (Pickering et al., 2016), the following analysis will be based on the criterion of $CRF \geq 90\%$ considering the contamination by low and mid-level NO_2 and comparisons with the results of Pickering et al. (2016) and ~~Lapierre et al. (2019)~~ Lapierre et al. (2020).

3.2 Comparison of LNO_x Production based on Different AMFs

~~Lapierre et al. (2019)~~ Lapierre et al. (2020) derived LNO_2 production based on the BEHR NO_2 product. In order for our results to be comparable with those of Pickering et al. (2016) and ~~Lapierre et al. (2019)~~ Lapierre et al. (2020), we choose NO_2 instead of NO_x to derive production per flash (production efficiency, PE). In Fig. 3, time series of NO_2 Vis, LNO_2 Vis, LNO_2 and LNO_2 Clean production per day over CONUS are plotted for MJJA 2014 with the criterion of $CRF \geq 90\%$ and a flash threshold of 2400 flashes per 2.4 h. ~~LNO_2 production values PEs~~ are mostly in the range from 20 to 80 mol/flash. ~~LNO_2 Vis productions PEs~~ are smaller than ~~LNO_2 productions PEs~~ which contain LNO_2 below clouds. The simulation of GMI in Pickering et al. (2016) indicated that 25% – 30% of the LNO_x column lies below the CP, while the ratio in our WRF-Chem simulation is $56 \pm 20\%$. The effect of cloud properties on LNO_x ~~production PE~~ will be discussed in more detail in section 3.4. Generally, the order of estimated daily PEs is LNO_2 Clean > LNO_2 > NO_2 Vis > LNO_2 Vis. The percent difference in the estimated PE (ΔPE) between NO_2 Vis and LNO_2 Vis indicates a certain amount of background NO_2 exists above clouds. Overall, the tendency of that ΔPE is consistent with another ΔPE between NO_2 Vis and LNO_2 Clean. When the region is highly polluted (ΔPE between NO_2 Vis and LNO_2 Vis is larger than 200%), PEs based on NO_2 Vis and LNO_2 Clean are significantly overestimated. In other words, NO_2 Vis and LNO_2 Clean are more sensitive to background NO_2 . The extent of the overestimation of NO_2 Vis is larger than that of LNO_2 Clean in highly polluted regions, while it is usually opposite in most regions.

Figure 4 shows the linear regression for ENTLN data versus NO_2 Vis, LNO_2 Vis, LNO_2 and LNO_2 Clean with the same criteria as shown in Fig. 3. LNO_2 Clean ~~production PE~~ (the largest slope) is 25.2 ± 22.3 mol NO_2 /flash with a correlation of 0.25 and 2.3 ± 2.1 mol NO_2 /stroke with a correlation of 0.22. As shown in Fig. 3, ~~the number of~~ positive percent differences

between NO₂Vis [PE](#) and LNO₂Clean ~~production is PE occur~~ much fewer than ~~that of~~ negative differences. As a result, NO₂Vis ~~production PE~~ (17.1 ± 17.2 mol NO₂/flash and 0.4 ± 1.0 mol NO₂/stroke) is smaller than LNO₂Clean ~~production PE~~ using the linear regression method.

~~If In order to compare our result with that of Lapierre et al. (2020), we tried to remove~~ the CP ≤ 650 hPa, TL ≥ 1000 and ratio ≥ 50% ~~are removed from criteria conditions from criteria.~~ But, our result based on daily summed NO₂Vis values (3.8 ± 0.5 mol/stroke) is still larger than the value of 1.6 ± 0.1 mol/stroke mentioned in ~~Lapierre et al. (2019)~~ [Lapierre et al. \(2020\)](#). This may be caused by the different version of BEHR algorithm, as ~~Lapierre et al. (2019)~~ [Lapierre et al. \(2020\)](#) used BEHR V3.0A and our algorithm is based on BEHR V3.0B (Laughner et al., 2019). The input of S_{NO_2} in both versions is from the NASA standard product V3 and the major improvements of BEHR V3.0B are listed below:

1. The profile (V3.0B) closest to the OMI overpass time was selected instead of the last profile (V3.0A) before the OMI overpass.
2. The AMF uses a variable tropopause height as opposed to the fixed 200 hPa tropopause.
3. The surface pressure is now calculated according to Zhou et al. (2009).

The detailed log of changes is available at <https://github.com/CohenBerkeleyLab/BEHR-core> (last access: March 8, 2020). Note that ~~Lapierre et al. (2019)~~ [Lapierre et al. \(2020\)](#) used the monthly NO₂ profile, while the daily profile is used in our study and the interval of our outputs from WRF-Chem is 30 min which is more frequent than 1 h in the BEHR daily product, the AMF could be affected by different NO₂ profiles. In view of these factors, we compare different methods based on our data to minimize these effects.

Meanwhile, LNO₂ ~~production PE~~ (18.7 ± 18.1 mol/flash and 2.1 ± 1.8 mol/stroke) is between LNO₂Clean ~~production PE~~ and NO₂Vis ~~production PE~~, which coincides with the daily results in Fig. 3. Furthermore, the ~~calculated LNO_x production based on PE based on the linear regression of~~ daily summed values ~~(not shown)~~, ~~the same method used in Pickering et al. (2016)~~, is 114.8 ± 18.2 mol/flash (or 17.8 ± 2.9 mol/stroke) which is larger than 91 mol/flash ~~from the linear regression result of in~~ Pickering et al. (2016), possibly due to the differences in geographic location, lightning data and chemistry model ~~considered by Pickering et al. (2016) and this study.~~

The mean and standard deviation of LNO₂ ~~production PE~~ under CRF ≥ 90% using the summation method is 46.2 ± 35.1 mol/flash and 9.9 ± 8.1 mol/stroke, while LNO_x ~~production PE~~ is 125.6 ± 95.9 mol/flash and 26.7 ± 21.6 mol/stroke (Fig. 5). The LNO₂ ~~PE~~ and LNO_x ~~production PE~~ are both higher in the Southeast U.S. (denoted by the red box in Fig. 5 panels, 75°W – 95°W, 25°N – 37°N), consistent with ~~Lapierre et al. (2019)~~ [Lapierre et al. \(2020\)](#) and Bucsela et al. (2019). Compared with Fig. 3, Figure 6a and b present some large differences between NO₂Vis ~~production PE~~ and LNO₂Vis ~~production PE~~, which are consistent with what we expect for polluted regions. Meanwhile, the differences between LNO₂ ~~production PE~~ and NO₂Vis ~~production PE~~ depend on background NO₂, the strength of updraft and the profile. The negative differences are caused by background NO₂ carried by the updraft while parts of the below-cloud LNO₂ ~~results in more result in LNO₂ production estimates PE higher~~ than NO₂Vis ~~production estimates PE~~ (Fig. 6c). Figure 6d shows that the ratio of LNO₂Vis to LNO₂ ranges from 10% – 80%. This may be caused by the height of the clouds and the profile of LNO₂. If the CP is near 300 hPa, the ratio should be smaller because of the coverage of clouds. ~~The ratio would also be smaller while~~ ~~While~~ peaks of the LNO₂ profile

are below the CP, the ratio would also be smaller. Therefore, a better understanding of LNO₂ profile and LNO_x below clouds
 320 is required.

3.3 Effects of Tropospheric Background on LNO_x Production

The With respect to the LNO₂ production, the patterns in Fig. 6 indicate the improvement of our approach is different in
 polluted and clean regions. To simplify the quantification, we select six grids with similar NO₂ profile (~ 100 pptv) above
 the cloud with CRF = 100%. These grid boxes contain the polluted and clean cities denoted by stars and triangles in Fig. 6a,
 325 respectively. Then, the differences between AMFs are dependent on fewer parameters:

$$AMF_{LNO_2} = \frac{\int_{p_{cloud}}^{p_{vp}} w_{cloudy}(p) NO_2(p) dp}{\int_{p_{surf}}^{p_{vp}} LNO_2(p) dp} \quad (7)$$

$$AMF_{NO_2Vis} = \frac{\int_{p_{cloud}}^{p_{vp}} w_{cloudy}(p) NO_2(p) dp}{\int_{p_{cl}}^{p_{vp}} NO_2(p) dp} \quad (8)$$

$$AMF_{LNO_2Clean} = \frac{\int_{p_{cloud}}^{p_{vp}} w_{cloudy}(p) LNO_2(p) dp}{\int_{p_{surf}}^{p_{vp}} LNO_2(p) dp} \quad (9)$$

Figure 7 compares the mean profiles of NO₂, background NO₂ and background NO₂ ratio in polluted and clean grids.
 330 Generally, the profiles of the ratio of background NO₂ ratio-over total NO₂ are C-shape because UT LNO₂ concentrations are
 higher than UT background NO₂ in-the-UT concentrations. However, the ratio profile in Fig. 7e has one peak between the cloud
 pressure and tropopause as background NO₂ increases and LNO₂ decreases. Besides, the percentage of UT background NO₂
 in polluted regions is steady and higher than that in clean regions.

Table 4 presents the relative changes among three methods in six cities. The difference between AMF_{LNO₂} (Eq. 7) and
 335 AMF_{LNO₂Clean} (Eq. 9) is the numerator: $\int_{p_{cloud}}^{p_{vp}} w_{cloudy}(p) NO_2(p) dp$ and $\int_{p_{cloud}}^{p_{vp}} w_{cloudy}(p) LNO_2(p) dp$. When the ratio of
 LNO₂ is higher or the region is cleaner, the relative difference is smaller (e.g. 5.0% – 12.0%, Fig. 7d – f). The largest relative
 difference (46.3%) occurs when the ratio of background NO₂ is continuously high in the UT (Fig. 7c). As a result, our approach
 is less sensitive to background NO₂ and more suitable for convections-convective cases over polluted locations. In contrast,
 production estimated by our method is larger than that based on NO₂Vis due to the LNO₂ below the cloud. When the cloud
 340 is higher, especially the peak of LNO profile is lower than the cloud (Fig. 7b), the relative difference is larger (121.2%)
 because more LNO₂ can not be included into the NO₂Vis, which has been discussed in Sect. 3.2. The relative change between
 AMF_{LNO₂Clean} (Eq. 9) and AMF_{NO₂Vis} (Eq. 8) depends on $\int_{p_{cloud}}^{p_{vp}} w_{cloudy}(p) LNO_2(p) dp / \int_{p_{surf}}^{p_{vp}} w_{cloudy}(p) LNO_2(p) dp$, which
 is also affected by cloud not the background NO₂. The largest relative change is (153.8% among the six grids where the highest
clouds occur) occurs at New Orleans, which has the lowest cloud pressure and consequently the smallest visible column.

345 3.4 Effects of Cloud and LNO_x Parameterization on LNO_x Production

Figure 8a presents the daily distribution of CP and the ratio of LNO₂Vis to LNO₂ during MJJA 2014 with the criteria defined in section 3.1 under CRF \geq 90%. Since the ratio of LNO₂Vis to LNO₂ decreases from 0.8 to 0.2 as the cloud pressure decreases from 600 to 300 hPa, NO₂Vis production-PE is smaller than LNO₂ PE in relatively clean areas as shown in Fig. 4. Apart from LNO₂Vis, the LNO₂ production-PE is also affected by CP. For LNO₂ production-PEs larger than 30 mol/stroke, the CPs are all smaller than 550 hPa (Fig. 8b). However, smaller LNO₂ production-PEs (< 30 mol/stroke) ~~occurs~~ occur on all levels between 650 hPa and 200 hPa. Because of the limited amount of large LNO₂ production-PEs and lightning data, we cannot derive the relationship between LNO₂ production-PE and cloud pressure or ~~different~~ other lightning properties at this stage. Because the CP only represents the development of clouds, the vertical structure of flashes can not be derived from the CP values only. As discussed in several previous studies, the flash channel length varies and depends on the environmental conditions (Carey et al., 2016; Mecikalski and Carey, 2017; Fuchs and Rutledge, 2018). Davis et al. (2019) compared two kinds of ~~flashes~~ flash: normal flashes and anomalous flashes. Because updrafts are stronger and flash rates are higher in anomalous storms, UT LNO_x concentrations ~~is~~ are larger in anomalous than normal polarity storms. In general, normal flashes are coupled with an upper-level positive charge region and a mid-level negative charge region, while anomalous flashes are opposite (Williams, 1989). It is not straightforward to estimate the error resulting from the vertical distribution of LNO_x. There are mainly two methods of distributing LNO_x in models: LNO_x profiles (postconvection) in which LNO_x has already been redistributed by convective transport, while the other one (preconvection) uses LNO_x production profiles made before the redistribution of convective transport (Allen et al., 2012; Luo et al., 2017). However, given the similarity of results compared to other LNO_x studies, we believe that our 1° × 1° results based on postconvective LNO_x profile are sufficient for estimating average LNO_x production.

The LNO production settings in WRF-Chem varied in different studies. Zhao et al. (2009) set a NO_x production rate of 250 mol NO per flash in a regional-scale model, while Bela et al. (2016) chose ~~the same value (330 mol NO per flash)~~ that was used by Barth et al. (2012). Wang et al. (2015) assumed approximately 500 mol NO per flash which was derived by a cloud-scale chemical transport model and in-cloud aircraft observations (Ott et al., 2010). To illustrate the impact of LNO_x parameterization on LNO_x estimation, we apply another WRF-Chem NO₂ profile setting (2×base flashrate, 500 mol NO flash⁻¹; hereinafter referred to as "2×500 mol NO flash⁻¹") to a priori profiles and evaluate the changes in AMF_{LNO₂}, AMF_{LNO_x}, LNO₂ PE and LNO_x productionsPE. For the linear regression method (Fig. 9), LNO₂ production-PE is 29.8 ± 20.5 mol/flash which is 59.4% larger than the basic one (18.7 ± 18.1 mol/flash). Meanwhile, LNO_x production-PE (increasing from 54.5 ± 48.1 mol/flash to 88.5 ± 61.1 mol/flash) also depends on the configuration of LNO production in WRF-Chem. The comparison between Fig. 4 and Fig. 9 shows that LNO₂Clean PE and LNO₂ PE are more similar while LNO₂ PE and NO₂Vis PE present the same tendency. It remains unclear as to whether the NO-NO₂-O₃ cycle or other LNO_x reservoirs accounts for the increment of LNO_x productionPE. This would need detailed source analysis in WRF-Chem and is beyond the scope of this study.

Figure 10 shows the average percentage changes in AMF_{LNO₂}, AMF_{LNO_x}, LNO₂ and LNO_x between retrievals using profiles based on 1×200 mol NO flash⁻¹ and 2×500 mol NO flash⁻¹. These results were obtained by averaging data over MJJA 2014 based on the method described in Sect. 2.5 with the criterion of CRF \geq 90%. The effects on LNO₂ and LNO_x retrieval from

increasing LNO profile values show mostly the same tendency: smaller AMF_{LNO_2} and AMF_{LNO_x} leads to larger LNO_2 and LNO_x , but the changes are regionally dependent. This is caused by the nonlinear calculation of AMF_{LNO_2} and AMF_{LNO_x} . As the contribution of LNO_2 increases, both the numerator and denominator of Eq. (2) increase. Note that the LNO_2 accounts for a fraction of NO_2 above the clouds, the magnitude of increasing denominator could be different than that of increasing numerator, resulting in a different effect on the AMF_{LNO_2} and AMF_{LNO_x} . As mentioned in Zhu et al. (2019), the lightning densities in the Southeast U.S. might be overestimated using the 2×500 mol NO flash⁻¹ setting and the same lightning parameterization as ours. Fortunately, the AMFs and estimated LNO_2 change little in that region. Because the Southeast U.S. has the highest flash density (Fig. 2), the NO_2 in the numerator of AMF is dominated by LNO_2 . Both the SCD and VCD will increase when the model uses higher LNO_2 . In other words, the sensitivity to the LNO setting decreases and the relative distribution of LNO_2 matters.

Figure 11 shows the comparison of the mean LNO and LNO_2 profiles in two specific regions where the 2×500 mol NO flash⁻¹ setting leads to both lower and higher LNO_2 production PEs, respectively. The first one (Fig. 11a) is the region ($36^\circ N - 37^\circ N$, $89^\circ W - 90^\circ W$) containing the minimal negative percent change in LNO_2 (Fig. 10c). The second one ($31^\circ N - 32^\circ N$, $97^\circ W - 98^\circ W$), Figure 11b, has the largest positive percent change in LNO_2 (Fig. 10c). Although the relative distributions of mean LNO and LNO_2 profiles are similar in both regions, the magnitude differs with a factor of 10. This phenomenon implies that the performance of lightning parameterization in WRF-Chem is region-regionally dependent and an unrealistic profile could appear in the UT. Although this sensitivity analysis is false in some regions, it allows the calculation of an upper limit on the NO_2 due to LNO and LNO_2 profiles. As discussed in Laughner and Cohen (2017), the scattering weights are uniform under cloudy conditions and the sensitivity of NO_2 is nearly constant with different pressure levels because of the high albedo. However, the relative distribution of LNO_2 within the UT should be taken carefully into consideration. If the LNO_2/NO_2 above the cloud is large enough (Fig. 11a), the AMF_{LNO_2} is largely determined by the ratio of LNO_2 Vis to LNO_2 which is related to the relative distribution. When the condition of high LNO_2/NO_2 is not met, both relative distribution and ratio are important (Fig. 11b).

To clarify this, we applied the same sensitivity test of different simulating LNO amounts for all four methods mentioned in Sect. 2.4: LNO_2 , LNO_2 Vis, LNO_2 Clean and NO_2 Vis (Fig. 12). Note that the threshold for CRF is set to 100% to simplify Eq. (2) to Eq. (7). The overall differences of LNO_2 Clean and NO_2 Vis are smaller than those of LNO_2 and LNO_2 Vis. Comparing the composition of numerator and denominator in the equations, it is clear why the impact of different simulating LNO amounts is smaller in Fig. 12c and d. For LNO_2 Clean and NO_2 Vis, both the SCD and VCD will increase (decrease) when more (less) LNO_2 or NO_2 presents. The difference between Fig. 12a and Fig. 12b is the denominator: the total tropospheric LNO_2 vertical column and visible LNO_2 vertical column respectively. As a result, the negative values in Fig. 12a is are caused by the part of LNO_2 below the cloud. The comparison between Fig. 4 and Fig. 9 shows that LNO_2 Clean and LNO_2 values are more similar while LNO_2 and NO_2 Vis values are same. The uncertainty of retrieved LNO_2 and LNO_x productions PEs is driven by this error, and we conservatively estimate this to be $\pm 1513\%$ and $\pm 2925\%$ respectively.

4 Uncertainties Analysis

The uncertainties of the LNO₂ and LNO_x ~~production-PEs~~ are estimated following Pickering et al. (2016), Allen et al. (2019), Bucselo et al. (2019), ~~Lapierre et al. (2019) and Laughner et al. (2019)~~ Laughner et al. (2019) and Lapierre et al. (2020). We
415 determine the uncertainty due to BEHR tropopause pressure, cloud radiance fraction, cloud pressure, surface pressure, surface reflectivity, profile shape, profile location, V_{strat}, the detection efficiency of lightning, t_{window} and LNO₂ lifetime numerically by perturbing each parameter in turn and ~~re-retrieval-of~~ re-retrieving the LNO₂ and LNO_x with the perturbed values (Table 5).

The GEOS-5 monthly tropopause pressure, which is consistent with the NASA Standard Product, is applied instead of the variable WRF tropopause height to evaluate the uncertainty (6% for LNO₂ PE and 4% for LNO_x PE) caused by the BEHR
420 tropopause pressure. ~~Beirle et al. (2009) obtained a mean total sensitivity of 0.46 (σ = 0.09) for LNO_x in the sensitivity study;~~ The cloud pressure bias is given as a function of cloud pressure and fraction by Acarreta et al. (2004) implying an uncertainty of 23% due to cloud pressure in our study 32%, the most likely uncertainty in the production analysis, for LNO₂ PE and 34% for LNO_x PE. The resolution of GLOBE terrain height data is much higher than the OMI pixel and a fixed scale height is assumed in the BEHR algorithm. As a result, Laughner et al. (2019) compared the average WRF surface pressures to the GLOBE surface
425 pressures and arrived at the largest bias of 1.5%. Based on the largest bias, we vary the surface pressure (limited to less than 1020 hPa) and the uncertainty can be neglected.

The error in cloud radiance fraction is transformed from cloud fraction using:

$$\sigma = 0.05 \cdot \left. \frac{\partial f_r}{\partial f_g} \right|_{f_{g, pix}} \quad (10)$$

where f_r is the cloud radiance fraction, f_g is the cloud fraction and $f_{g, pix}$ is the cloud fraction of a specific pixel. We calculate
430 $\partial f_r / \partial f_g$ under $f_{g, pix}$ by the relationship between all binned f_r and f_g with the increment of 0.05 for the each specific OMI orbit. Considering the relationship, the error in cloud fraction is converted to an error in cloud radiance fraction of 2% for ~~both~~ the LNO₂ and LNO_x PEs.

The accuracy of the 500 m MODIS albedo product is usually within 5% of albedo observations at the validation sites and those exceptions with low quality flags have been found to be primarily within 10% of the field data (Schaaf et al., 2011). Since
435 we use the bidirectional reflectance distribution function (BRDF) data directly, rather than including a radiative transfer model, 14% Lambertian equivalent reflectivity (LER) error and 10% uncertainty are combined to get a perturbation of 17% (Laughner et al., 2019). The uncertainty due to surface reflectivity can be neglected with the 17% perturbation.

As discussed at the end of Sect. 3.4, another setting of LNO₂ ($2 \times 500 \text{ mol NO flash}^{-1}$) is applied to determine the uncertainty of the lightning parameterization and the vertical distribution of LNO in WRF-Chem. Differences between the two profiles
440 lead to an uncertainty of ~~15% and 29~~ 13% and 25% in the resulting PEs of LNO₂ and LNO_x production. Another sensitivity test allows each pixel to shift by - 0.2, 0, or + 0.2 degrees in the directions of longitude and latitude, taking advantage of the high-resolution profile location in WRF-Chem. The resulting uncertainty of LNO_x production-PE is 1% including the error of transport and chemistry by shifting pixels.

Compared to the NASA standard product v2, Krotkov et al. (2017) demonstrated that the noise in V_{strat} is $1 \times 10^{14} \text{ cm}^{-2}$.
445 Errors in polluted regions can be slightly larger than this value, while errors in the cleanest areas are typically significantly smaller (Bucsela et al., 2013). We estimated the uncertainty of V_{strat} component and the slant column errors to be 10% and 5%, respectively, following Allen et al. (2019).

Based on the standard deviation of the detection efficiency estimation over the CONUS relative to LIS, ENTLN detection efficiency uncertainties are $\pm 16\%$ for total and IC flashes/strokes. Due to the high detection efficiency of CG over the CONUS,
450 the uncertainty is estimated to be $\pm 5\%$ (Lapierre et al., 2019)(Lapierre et al., 2020). It is found that the resulting uncertainty of detection efficiency is 15% in the production analysis. We have used the t_{window} of 2.4 h for counting ENTLN flashes and strokes to analyze LNO_2 and LNO_x production. Because t_{window} derived from the ERA5 reanalysis can not represent the variable wind speeds, a sensitivity test is performed which yields an uncertainty of 10% for production per flash and 8% for production per stroke using t_{window} of 2 h and 4 h. Meanwhile, the lifetime of UT NO_x ranges from 2 hours to 12 hours depending on the
455 convective location, the methyl peroxy nitrate and alkyl and multifunctional nitrates (Nault et al., 2017). The lifetime (τ) of NO_2 in Eq. (6) is replaced by 2 and 12 hours to determine the uncertainty as 24% due to lifetime. ~~The lifetime is the most likely uncertainty in the production analysis of LNO_2 while the uncertainty~~ This is comparable with the uncertainty (25%) caused by lightning parameterization ~~is comparable with that~~ for the LNO_x type.

Recent works revealed that the modeled NO/NO_2 ratio departs from the data in the SEAC⁴RS aircraft campaign (Travis
460 et al., 2016; Silvern et al., 2018). Silvern et al. (2018) attributed this to the positive interference on the NO_2 measurements or errors in the cold-temperature $\text{NO}-\text{NO}_2-\text{O}_3$ photochemical reaction rate. We assign ~~an uncertainty of a 20% bias with $\pm 15\%$ uncertainty~~ to this error considering the possible positive NO_2 measurements interferences (Allen et al., 2019; Bucsela et al., 2019) and estimate the uncertainty to be 15% for LNO_x PE.

In addition, the estimation of LNO_x PE ~~is also dependent~~ also depends on the tropospheric background NO_2 . In our method,
465 main factors affecting this factor are the emissions inventory and the amount of transported NO_2 . For the emissions inventory, the sources of uncertainty are assumptions, methods, input data and calculation errors. As a result, the uncertainties for different species or pollutants related to NO_2 are different and EPA also doesn't publish the quantified uncertainty measures because the parties that submit emissions estimates to EPA are not asked to include quantitative uncertainty measurements or estimates (EPA, 2015). For the simulated convective transport, Li et al. (2018) compared the cloud-resolving simulations with these
470 based on convective parameterization and pointed out that the convective transport was weaker in the parameterization. But, we believe that the ratio condition ($\text{LNO}_2/\text{Vis}/\text{NO}_2/\text{Vis} \geq 50\%$) should reduce these two kinds of uncertainty and assume an uncertainty of 10%, which is less than 20% assigned in Allen et al. (2019) and Bucsela et al. (2019).

The overall uncertainty is estimated as the square root of the sum of the squares of all individual uncertainties in Table 5. The net uncertainty is 48% and ~~54~~56% for LNO_2 type and LNO_x type respectively. The mean $\text{LNO}_2/\text{flash}$, $\text{LNO}_x/\text{flash}$,
475 $\text{LNO}_2/\text{stroke}$, $\text{LNO}_x/\text{stroke}$ based on the linear regression and summation method are 32 mol/flash, 90 mol/flash, 6 mol/stroke and 17 mol/stroke. Applying the corresponding uncertainty to these mean values, we arrive at 32 ± 15 mol $\text{LNO}_2/\text{flash}$, 90 ± 49 50 mol $\text{LNO}_x/\text{flash}$, 6 ± 3 mol $\text{LNO}_2/\text{stroke}$ and 17 ± 9 10 mol $\text{LNO}_x/\text{stroke}$. This is in the range of current literature estimate ranging from 33 to 500 mol $\text{LNO}_x/\text{flash}$ (Schumann and Huntrieser, 2007; Beirle et al., 2010; Bucsela et al., 2010).

Bucsela et al. (2010) estimated LNO_x ~~production-PE~~ of 100 – 250 mol/flash which is ~~similar to our flash-based results~~ higher than but overlaps with our estimate. Pickering et al. (2016) estimated LNO_x ~~production-PE~~ to be 80 ± 45 mol per flash for the Gulf of Mexico, ~~which~~. This is 50% smaller than our flash-based results over the CONUS, if we use the same linear regression method which is based on the daily summed values instead of daily mean values. Note that the criteria defined in Sect. 3.1 lead to many missing data over the Gulf of Mexico, thus it is actually a comparison between different regions. For the stroke-based results, ~~Lapierre et al. (2019)~~ Lapierre et al. (2020) yields lower LNO₂ ~~production-PE~~ of 1.6 ± 0.1 mol per stroke, the difference is caused by the different version of BEHR algorithm and several settings as mentioned in Sect. 3.2. Bucsela et al. (2019) inferred an average value of 200 ± 110 moles (~~67~~ 122% larger than our results) LNO_x produced per flash over the North America, this is related to the different algorithm ~~and lightning data~~, lightning data and lightning thresholds.

5 Conclusions

In this study, a new algorithm for retrieving LNO₂ (LNO_x) from OMI, including LNO₂ (LNO_x) below cloud, has been developed for application over active convection. It works in both clean and polluted regions because of the consideration of tropospheric background pollution in the definition of AMFs. It uses specific criteria combining with several other conditions (sufficient CRF, coincident ENTLN data, TL ≥ 1000 and ratio ≥ 50%) to ensure that the electrically active regions are detected by OMI and simulated by WRF-Chem successfully. We conducted an analysis on 1° × 1° daily boxes in MJJA 2014 and obtained the seasonal mean LNO₂ and LNO_x production efficiencies over the CONUS. Considering all the uncertainties (Table 5) and applying the summation and regression method, the final mean production efficiencies are estimated to be 32 ± 15 mol LNO₂/flash, 90 ± ~~49~~ 50 mol LNO_x/flash, 6 ± 3 mol LNO₂/stroke and 17 ± ~~9~~ 10 mol LNO_x/stroke.

Compared with ~~former methods, our method has reduced the sensitive to background NO₂, while the method in Lapierre et al. (2019) underestimates LNO_x production efficiency because of the neglected~~ Lapierre et al. (2020), we find that the LNO₂ production could be larger when the below-cloud LNO₂ ~~and LNO₂ production is overestimated using the method in Pickering et al. (2016) due to the over-cloud is taken into account, especially for the high clouds. Meanwhile, if the method of Pickering et al. (2016) is applied without the~~ background NO₂ ~~in correction, the derived LNO_x production efficiency is similar to ours in clean regions or regions with high LNO₂ concentration above the cloud, but it could be overestimated more than 18% in~~ polluted regions. Finally, implementing profiles generated with different model settings of lightning (1 × 200 mol NO flash⁻¹ and 2 × 500 mol NO flash⁻¹), we find that the larger LNO production ~~model~~-setting leads to 62% larger retrieval of LNO_x on average despite some regionally dependent effects caused by the nonlinear calculation of AMF. Both the ratio of the tropospheric LNO₂ above the cloud to the total tropospheric LNO₂ and the ratio of LNO₂ to NO₂ cause different comprehensive effects due to the nonlinear calculation of AMF_{LNO₂} and AMF_{LNO_x}.

Since other regions, like China and India, have much more NO₂ pollution than the CONUS, it is necessary to consider the background NO₂ in detail. These analyses will be complemented by the recently launched satellite instrument (TROPOspheric Monitoring Instrument [TROPOMI]) (Veefkind et al., 2012; Boersma et al., 2018; Griffin et al., 2019) and Lightning Mapping Imager (LMI) on the new generation Chinese geostationary meteorological satellites Fengyun-4 (Min et al., 2017; Yang et al.,

2017; Zhang et al., 2019). Future work investigating the flash channel length and more detailed lightning parameterization in WRF-Chem would greatly benefit LNO_x estimation. Applying current method in future studies may enhance the accuracy of LNO_x production at both local and global scales.

515 *Code and data availability.* The retrieval algorithm used in Sect. 2.4 is available at <https://github.com/zxdawn/BEHR-LNOx> (last access: March 8, 2020; Zhang and Laughner, 2019). The WRF-Chem model output and LNO_x product are available upon request to Xin Zhang (xinzhang1215@gmail.com).

Appendix A: AMF Definitions used in this Study

$$AMF_{LNO_2} = \frac{(1 - f_r) \int_{p_{surf}}^{p_{tp}} w_{clear}(p) NO_2(p) dp + f_r \int_{p_{cloud}}^{p_{tp}} w_{cloudy}(p) NO_2(p) dp}{\int_{p_{surf}}^{p_{tp}} LNO_2(p) dp} \quad (A1)$$

$$520 \quad AMF_{LNO_x} = \frac{(1 - f_r) \int_{p_{surf}}^{p_{tp}} w_{clear}(p) NO_2(p) dp + f_r \int_{p_{cloud}}^{p_{tp}} w_{cloudy}(p) NO_2(p) dp}{\int_{p_{surf}}^{p_{tp}} LNO_x(p) dp} \quad (A2)$$

where f_r is the [radiance-cloud-cloud radiance](#) fraction, p_{surf} is the surface pressure, p_{tp} is the tropopause pressure, p_{cloud} is the cloud optical pressure (CP), w_{clear} and w_{cloudy} are respectively the pressure dependent scattering weights from the TOMRAD lookup table (Bucsela et al., 2013) for clear and cloudy parts, and $NO_2(p)$ is the modeled NO₂ vertical profile. $LNO_2(p)$ and $LNO_x(p)$ are respectively the LNO₂ and LNO_x vertical profile calculated by the difference of vertical profiles between
525 WRF-Chem simulations with and without lightning.

$$AMF_{LNO_2Clean} = \frac{(1 - f_r) \int_{p_{surf}}^{p_{tp}} w_{clear}(p) LNO_2(p) dp + f_r \int_{p_{cloud}}^{p_{tp}} w_{cloudy}(p) LNO_2(p) dp}{\int_{p_{surf}}^{p_{tp}} LNO_2(p) dp} \quad (A3)$$

$$AMF_{NO_2Vis} = \frac{(1 - f_r) \int_{p_{surf}}^{p_{tp}} w_{clear}(p) NO_2(p) dp + f_r \int_{p_{cloud}}^{p_{tp}} w_{cloudy}(p) NO_2(p) dp}{(1 - f_g) \int_{p_{surf}}^{p_{tp}} NO_2(p) dp + f_g \int_{p_{cloud}}^{p_{tp}} NO_2(p) dp} \quad (A4)$$

$$AMF_{NO_xVis} = \frac{(1 - f_r) \int_{p_{surf}}^{p_{tp}} w_{clear}(p) NO_2(p) dp + f_r \int_{p_{cloud}}^{p_{tp}} w_{cloudy}(p) NO_2(p) dp}{(1 - f_g) \int_{p_{surf}}^{p_{tp}} NO_x(p) dp + f_g \int_{p_{cloud}}^{p_{tp}} NO_x(p) dp} \quad (A5)$$

$$AMF_{LNO_2Vis} = \frac{(1 - f_r) \int_{p_{surf}}^{p_{tp}} w_{clear}(p) NO_2(p) dp + f_r \int_{p_{cloud}}^{p_{tp}} w_{cloudy}(p) NO_2(p) dp}{(1 - f_g) \int_{p_{surf}}^{p_{tp}} LNO_2(p) dp + f_g \int_{p_{cloud}}^{p_{tp}} LNO_2(p) dp} \quad (A6)$$

530 where f_g is the geometric cloud fraction and $NO_x(p)$ is the modeled NO_x vertical profile.

Appendix B: LNO_x Production based on Lower Lightning Thresholds

535 While we used 2400 flashes box⁻¹ and 8160 strokes box⁻¹ per 2.4 hour time window for detecting LNO_x, here we show results obtained when using 1 flash box⁻¹ and 3.4 strokes box⁻¹ in the same time window. We note that the WRF total lightning threshold is also reduced to 1 flash box⁻¹, but we keep the ratio condition unchanged. Briefly, the condition is CRF90_ENTLN1(3.4)_TL1_ratio50 as shown in Table 1.

Similarly, the order of estimated daily PEs is LNO₂Clean > LNO₂ > NO₂Vis > LNO₂Vis (Fig. B1). Compared with Fig. 4, the LNO₂ per flash and LNO_x per flash are larger while PEs based on stroke data are smaller. Considering the additional boxes of fewer lightning counts, differences in the daily mean flashes and NO_x results in different PEs and the relationship presents more like the power function as mentioned in Bucselá et al. (2019).

540 Instead of using the nonlinear regression of power function:

$$y = \alpha x^\beta \quad (\text{B1})$$

where x is flashes or strokes and y is NO₂ or NO_x, we take the logarithm of both sides and apply the linear regression to data:

$$\log_{10} y = \log_{10} \alpha + \beta \log_{10} x \quad (\text{B2})$$

545 As expected, the linear regression based on logarithmized data performs better in this situation and yields $\alpha = 38$ kmol, and $\beta = 0.3$ for LNO_x per flash (Fig. B2). Since we use the unbinned data (flashes not divided into many groups), we compare our results with Bucselá et al. (2019) based on the same kind of data ($\alpha = 10.3$ kmol, and $\beta = 0.42$). The large difference of α is related to the method of estimating LNO_x, different lightning data (WWLLN and ENTLN) and different regions (northern midlatitudes and CONUS). Note that the resolution (13×24 km²) of OMI could weaken the signal of LNO_x. We believe the phenomenon of higher production efficiency as flash rate decreases (Fig. B3) could be explored in much detail with higher resolution data like the TROPOMI data.

550

Author contributions. YY directed the research and RJvdA, XZ and YY designed the research with feedback from the other co-authors; RJvdA and XZ developed the algorithm; JLL provided guidance and supporting data on the ENTLN data; XZ performed simulations and analysis with the help of YY, RJvdA, QC, XK, SY, JC, CH and RS; YY, RJvdA, JLL and XZ interpreted the data and discussed the results. XZ drafted the manuscript with comments from the co-authors; JLL, RJvdA and YY edited the manuscript.

555 *Competing interests.* The authors declare that they have no conflict of interest.

Acknowledgements. This work was funded by the National Natural Science Foundation of China (91644224 and 41705118). We acknowledge use of the computational resource provided by the National Supercomputer Centre in Guangzhou (NSCC-GZ). We thank the University of California Berkeley Satellite Group for the basic BEHR algorithm. We also thank Earth Networks Company for providing the

Earth Networks Total Lightning Network (ENTLN) datasets. We appreciate the discussions with Joshua L. Laughner for BEHR codes and
560 Mary Barth for the WRF-Chem lightning NO_x module. MOZART-4 global model output is available at <https://www.aoml.ucar.edu/wrf-chem/mozart.shtml> (last access: March 8, 2020). ~~Finally, we thank the three anonymous reviewers whose detailed comments helped us improve and clarify~~ The authors would also like to thank all anonymous reviewers as well as Kenneth E. Pickering, Eric J. Bucsela and Dale J. Allen for detailed comments which greatly improved this manuscript. Finally, we thank all contributors of Python packages used in this paper (Met Office, 2010 - 2015; Hoyer and Hamman, 2017; Hunter, 2007; Jiawei Zhuang et al., 2019; McKinney, 2011; Inc., 2015; Seabold and Perktold, 2010)

565 ~

References

- Acarreta, J. R., de Haan, J. F., and Stammes, P.: Cloud pressure retrieval using the O₂ -O₂ absorption band at 477 nm, *Journal of Geophysical Research*, 109, 2165, <https://doi.org/10.1029/2003JD003915>, 2004.
- Allen, D. J., Pickering, K. E., Duncan, B. N., and Damon, M.: Impact of lightning NO emissions on North American photochemistry as determined using the Global Modeling Initiative (GMI) model, *Journal of Geophysical Research*, 115, 4711, <https://doi.org/10.1029/2010JD014062>, 2010.
- Allen, D. J., Pickering, K. E., Pinder, R. W., Henderson, B. H., Appel, K. W., and Prados, A.: Impact of lightning-NO on eastern United States photochemistry during the summer of 2006 as determined using the CMAQ model, *Atmospheric Chemistry and Physics*, 12, 1737–1758, <https://doi.org/10.5194/acp-12-1737-2012>, 2012.
- 575 Allen, D. J., Pickering, K. E., Bucseła, E. J., Krotkov, N., and Holzworth, R.: Lightning NO_x Production in the Tropics as Determined Using OMI NO₂ Retrievals and WLLN Stroke Data, *Journal of Geophysical Research: Atmospheres*, <https://doi.org/10.1029/2018JD029824>, 2019.
- Banerjee, A., Archibald, A. T., Maycock, A. C., Telford, P., Abraham, N. L., Yang, X., Braesicke, P., and Pyle, J. A.: Lightning NO_x, a key chemistry–climate interaction: impacts of future climate change and consequences for tropospheric oxidising capacity, *Atmospheric Chemistry and Physics*, 14, 9871–9881, <https://doi.org/10.5194/acp-14-9871-2014>, 2014.
- 580 Barth, M. C., Lee, J., Hodzic, A., Pfister, G., Skamarock, W. C., Worden, J., Wong, J., and Noone, D.: Thunderstorms and upper troposphere chemistry during the early stages of the 2006 North American Monsoon, *Atmospheric Chemistry and Physics*, 12, 11 003–11 026, <https://doi.org/10.5194/acp-12-11003-2012>, 2012.
- Beirle, S., Platt, U., Wenig, M., and Wagner, T.: NO_x production by lightning estimated with GOME, *Advances in Space Research*, 34, 793–797, <https://doi.org/10.1016/j.asr.2003.07.069>, 2004.
- 585 Beirle, S., Spichtinger, N., Stohl, A., Cummins, K. L., Turner, T., Boccippio, D., Cooper, O. R., Wenig, M., Grzegorski, M., Platt, U., and Wagner, T.: Estimating the NO_x produced by lightning from GOME and NLDN data: A case study in the Gulf of Mexico, *Atmospheric Chemistry and Physics*, 6, 1075–1089, <https://doi.org/10.5194/acp-6-1075-2006>, 2006.
- Beirle, S., Salzmann, M., Lawrence, M. G., and Wagner, T.: Sensitivity of satellite observations for freshly produced lightning NO_x, *Atmospheric Chemistry and Physics*, 9, 1077–1094, <https://doi.org/10.5194/acp-9-1077-2009>, 2009.
- 590 Beirle, S., Huntrieser, H., and Wagner, T.: Direct satellite observation of lightning-produced NO_x, *Atmospheric Chemistry and Physics*, 10, 10965–10986, <https://doi.org/10.5194/acp-10-10965-2010>, 2010.
- Bela, M. M., Barth, M. C., Toon, O. B., Fried, A., Homeyer, C. R., Morrison, H., Cummings, K. A., Li, Y., Pickering, K. E., Allen, D. J., Yang, Q., Wennberg, P. O., Crouse, J. D., St. Clair, J. M., Teng, A. P., O’Sullivan, D., Huey, L. G., Chen, D., Liu, X., Blake, D. R., Blake, N. J., Apel, E. C., Hornbrook, R. S., Flocke, F., Campos, T., and Diskin, G.: Wet scavenging of soluble gases in DC3 deep convective storms using WRF-Chem simulations and aircraft observations, *Journal of Geophysical Research: Atmospheres*, 121, 4233–4257, <https://doi.org/10.1002/2015JD024623>, 2016.
- 595 Boersma, K. F., Eskes, H. J., Meijer, E. W., and Kelder, H. M.: Estimates of lightning NO_x production from GOME satellite observations, *Atmospheric Chemistry and Physics*, 5, 2311–2331, <https://doi.org/10.5194/acp-5-2311-2005>, 2005.
- 600 Boersma, K. F., Eskes, H. J., Richter, A., de Smedt, I., Lorente, A., Beirle, S., van Geffen, J. H. G. M., Zara, M., Peters, E., van Roozendaal, M., Wagner, T., de Maasackers, J., van der A, R. J., Nightingale, J., de Rudder, A., Irie, H., Pinardi, G., Lambert, J.-C., and Compernelle, S. C.: Improving algorithms and uncertainty estimates for satellite NO₂ retrievals: results from the quality assurance for the essential

- climate variables (QA4ECV) project, *Atmospheric Measurement Techniques*, 11, 6651–6678, <https://doi.org/10.5194/amt-11-6651-2018>, 2018.
- 605 Bovensmann, H., Burrows, J. P., Buchwitz, M., Frerick, J., Noël, S., Rozanov, V. V., Chance, K. V., and Goede, A. P. H.: SCIAMACHY: Mission Objectives and Measurement Modes, *Journal of the Atmospheric Sciences*, 56, 127–150, [https://doi.org/10.1175/1520-0469\(1999\)056<0127:SMOAMM>2.0.CO;2](https://doi.org/10.1175/1520-0469(1999)056<0127:SMOAMM>2.0.CO;2), 1999.
- Browne, E. C., Wooldridge, P. J., Min, K.-E., and Cohen, R. C.: On the role of monoterpene chemistry in the remote continental boundary layer, *Atmospheric Chemistry and Physics*, 14, 1225–1238, <https://doi.org/10.5194/acp-14-1225-2014>, 2014.
- 610 Bucselá, E. J., Pickering, K. E., Huntemann, T. L., Cohen, R. C., Perring, A., Gleason, J. F., Blakeslee, R. J., Albrecht, R. I., Holzworth, R., Cipriani, J. P., Vargas-Navarro, D., Mora-Segura, I., Pacheco-Hernández, A., and Laporte-Molina, S.: Lightning-generated NO_x seen by the Ozone Monitoring Instrument during NASA's Tropical Composition, Cloud and Climate Coupling Experiment (TC⁴), *Journal of Geophysical Research*, 115, 793, <https://doi.org/10.1029/2009JD013118>, 2010.
- Bucselá, E. J., Krotkov, N. A., Celarier, E. A., Lamsal, L. N., Swartz, W. H., Bhartia, P. K., Boersma, K. F., Veefkind, J. P., Gleason, J. F., 615 and Pickering, K. E.: A new stratospheric and tropospheric NO₂ retrieval algorithm for nadir-viewing satellite instruments: Applications to OMI, *Atmospheric Measurement Techniques*, 6, 2607–2626, <https://doi.org/10.5194/amt-6-2607-2013>, 2013.
- Bucselá, E. J., Pickering, K. E., Allen, D. J., Holzworth, R., and Krotkov, N. A.: Midlatitude lightning NO_x production efficiency inferred from OMI and WLLN data, *Journal of Geophysical Research: Atmospheres*, <https://doi.org/10.1029/2019JD030561>, 2019.
- Burrows, J. P., Weber, M., Buchwitz, M., Rozanov, V., Ladstätter-Weissenmayer, A., Richter, A., DeBeek, R., Hoogen, R., Bramstedt, K., Eichmann, K.-U., Eisinger, M., and Perner, D.: The Global Ozone Monitoring Experiment (GOME): Mission Concept and First Scientific Results, *Journal of the Atmospheric Sciences*, 56, 151–175, [https://doi.org/10.1175/1520-0469\(1999\)056<0151:TGOMEG>2.0.CO;2](https://doi.org/10.1175/1520-0469(1999)056<0151:TGOMEG>2.0.CO;2), 1999.
- Callies, J., Corpaccioli, E., Eisinger, M., Hahne, A., and Lefebvre, A.: GOME-2-Metop's second-generation sensor for operational ozone monitoring, *ESA bulletin*, 102, 28–36, 2000.
- Carey, L. D., Koshak, W., Peterson, H., and Mecikalski, R. M.: The kinematic and microphysical control of lightning rate, extent, and NO_x 625 production, *Journal of Geophysical Research: Atmospheres*, 121, 7975–7989, <https://doi.org/10.1002/2015JD024703>, 2016.
- Choi, S., Joiner, J., Choi, Y., Duncan, B. N., Vasilkov, A., Krotkov, N., and Bucselá, E.: First estimates of global free-tropospheric NO₂ abundances derived using a cloud-slicing technique applied to satellite observations from the Aura Ozone Monitoring Instrument (OMI), *Atmospheric Chemistry and Physics*, 14, 10 565–10 588, <https://doi.org/10.5194/acp-14-10565-2014>, 2014.
- Clark, S. K., Ward, D. S., and Mahowald, N. M.: Parameterization-based uncertainty in future lightning flash density, *Geophysical Research Letters*, 44, 2893–2901, <https://doi.org/10.1002/2017GL073017>, 2017.
- 630 Davis, T. C., Rutledge, S. A., and Fuchs, B. R.: Lightning location, NO_x production, and transport by anomalous and normal polarity thunderstorms, *Journal of Geophysical Research: Atmospheres*, <https://doi.org/10.1029/2018JD029979>, 2019.
- DeCaria, A. J., Pickering, K. E., Stenichikov, G. L., Scala, J. R., Stith, J. L., Dye, J. E., Ridley, B. A., and Laroche, P.: A cloud-scale model study of lightning-generated NO_x in an individual thunderstorm during STERAO-A, *Journal of Geophysical Research*, 105, 11 601– 635 11 616, <https://doi.org/10.1029/2000JD900033>, 2000.
- DeCaria, A. J., Pickering, K. E., Stenichikov, G. L., and Ott, L. E.: Lightning-generated NO_x and its impact on tropospheric ozone production: A three-dimensional modeling study of a Stratosphere-Troposphere Experiment: Radiation, Aerosols and Ozone (STERAO-A) thunderstorm, *Journal of Geophysical Research*, 110, n/a–n/a, <https://doi.org/10.1029/2004JD005556>, 2005.

- Dobber, M., Kleipool, Q., Dirksen, R., Levelt, P., Jaross, G., Taylor, S., Kelly, T., Flynn, L., Leppelmeier, G., and Rozemeijer, N.: Validation of
640 Ozone Monitoring Instrument level 1b data products, *Journal of Geophysical Research*, 113, 5224, <https://doi.org/10.1029/2007JD008665>,
2008.
- Emmons, L. K., Walters, S., Hess, P. G., Lamarque, J.-F., Pfister, G. G., Fillmore, D., Granier, C., Guenther, A., Kinnison, D., Laepple, T.,
Orlando, J., Tie, X., Tyndall, G., Wiedinmyer, C., Baughcum, S. L., and Kloster, S.: Description and evaluation of the Model for Ozone and
645 Related chemical Tracers, version 4 (MOZART-4), *Geoscientific Model Development*, 3, 43–67, <https://doi.org/10.5194/gmd-3-43-2010>,
2010.
- EPA, U.: 2011 National Emissions Inventory, version 2—Technical support document, US Environmental Protection Agency, Office of Air
Quality Planning and Standards. Accessed August 2017., 2015.
- EPA, U. S. and OAR: Air Pollutant Emissions Trends Data | US EPA, [https://www.epa.gov/air-emissions-inventories/
air-pollutant-emissions-trends-data](https://www.epa.gov/air-emissions-inventories/air-pollutant-emissions-trends-data), 2015.
- 650 Finney, D. L., Doherty, R. M., Wild, O., Young, P. J., and Butler, A.: Response of lightning NO_x emissions and ozone production to
climate change: Insights from the Atmospheric Chemistry and Climate Model Intercomparison Project, *Geophysical Research Letters*, 43,
5492–5500, <https://doi.org/10.1002/2016GL068825>, 2016.
- Finney, D. L., Doherty, R. M., Wild, O., Stevenson, D. S., MacKenzie, I. A., and Blyth, A. M.: A projected decrease in lightning under
climate change, *Nature Climate Change*, 8, 210–213, <https://doi.org/10.1038/s41558-018-0072-6>, 2018.
- 655 Fried, A., Barth, M. C., Bela, M., Weibring, P., Richter, D., Walega, J., Li, Y., Pickering, K., Apel, E., Hornbrook, R., Hills, A., Riemer,
D. D., Blake, N., Blake, D. R., Schroeder, J. R., Luo, Z. J., Crawford, J. H., Olson, J., Rutledge, S., Betten, D., Biggerstaff, M. I.,
Diskin, G. S., Sachse, G., Campos, T., Flocke, F., Weinheimer, A., Cantrell, C., Pollack, I., Peischl, J., Froyd, K., Wisthaler, A., Mikoviny,
T., and Woods, S.: Convective transport of formaldehyde to the upper troposphere and lower stratosphere and associated scavenging in
thunderstorms over the central United States during the 2012 DC3 study, *Journal of Geophysical Research: Atmospheres*, 121, 7430–7460,
660 <https://doi.org/10.1002/2015JD024477>, 2016.
- Fuchs, B. R. and Rutledge, S. A.: Investigation of Lightning Flash Locations in Isolated Convection Using LMA Observations, *Journal of
Geophysical Research: Atmospheres*, 123, 6158–6174, <https://doi.org/10.1002/2017JD027569>, 2018.
- Goliff, W. S., Stockwell, W. R., and Lawson, C. V.: The regional atmospheric chemistry mechanism, version 2, *Atmospheric Environment*,
68, 174–185, <https://doi.org/10.1016/j.atmosenv.2012.11.038>, 2013.
- 665 Grell, G. A., Peckham, S. E., Schmitz, R., McKeen, S. A., Frost, G., Skamarock, W. C., and Eder, B.: Fully coupled “online” chemistry
within the WRF model, *Atmospheric Environment*, 39, 6957–6975, <https://doi.org/10.1016/j.atmosenv.2005.04.027>, 2005.
- Griffin, D., Zhao, X., McLinden, C. A., Boersma, F., Bourassa, A., Dammers, E., Degenstein, D., Eskes, H., Fehr, L., Fioletov, V., Hayden,
K., Kharol, S. K., Li, S.-M., Makar, P., Martin, R. V., Mihele, C., Mittermeier, R. L., Krotkov, N., Snee, M., Lamsal, L. N., Linden, M. t.,
van Geffen, J., Veefkind, P., and Wolde, M.: High-Resolution Mapping of Nitrogen Dioxide With TROPOMI: First Results and Validation
670 Over the Canadian Oil Sands, *Geophysical Research Letters*, 46, 1049–1060, <https://doi.org/10.1029/2018GL081095>, 2019.
- Guenther, A., Karl, T., Harley, P., Wiedinmyer, C., Palmer, P. I., and Geron, C.: Estimates of global terrestrial isoprene emissions using
MEGAN (Model of Emissions of Gases and Aerosols from Nature), *Atmospheric Chemistry and Physics*, 6, 3181–3210, [https://hal.
archives-ouvertes.fr/hal-00295995](https://hal.archives-ouvertes.fr/hal-00295995), 2006.
- Hauglustaine, D., Emmons, L., Newchurch, M., Brasseur, G., Takao, T., Matsubara, K., Johnson, J., Ridley, B., Stith, J., and Dye, J.: On the
675 Role of Lightning NO_x in the Formation of Tropospheric Ozone Plumes: A Global Model Perspective, *Journal of Atmospheric Chemistry*,
38, 277–294, <https://doi.org/10.1023/A:1006452309388>, 2001.

- Hoyer, S. and Hamman, J.: xarray: N-D labeled arrays and datasets in Python, *Journal of Open Research Software*, 5, <https://doi.org/10.5334/jors.148>, <http://doi.org/10.5334/jors.148>, 2017.
- Hunter, J. D.: Matplotlib: A 2D Graphics Environment, *Computing in Science & Engineering*, 9, 90–95, <https://doi.org/10.1109/MCSE.2007.55>, 2007.
- 680 Inc., P. T.: Collaborative data science, <https://plot.ly>, 2015.
- Jiawei Zhuang, Jiling, A., and Rasp, S.: JiaweiZhuang/xESMF: v0.2.1, <https://doi.org/10.5281/zenodo.1134365>, 2019.
- Joiner, J., Vasilkov, A. P., Gupta, P., Bhartia, P. K., Veefkind, P., Sneep, M., de Haan, J., Polonsky, I., and Spurr, R.: Fast simulators for satellite cloud optical centroid pressure retrievals; evaluation of OMI cloud retrievals, *Atmospheric Measurement Techniques*, 5, 529–545, <https://doi.org/10.5194/amt-5-529-2012>, 2012.
- 685 KNMI: Background information about the Row Anomaly in OMI, <http://projects.knmi.nl/omi/research/product/rowanomaly-background.php>, last access: March 8, 2020, 2012.
- Krause, A., Kloster, S., Wilkenskjeld, S., and Paeth, H.: The sensitivity of global wildfires to simulated past, present, and future lightning frequency, *Journal of Geophysical Research: Biogeosciences*, 119, 312–322, <https://doi.org/10.1002/2013JG002502>, 2014.
- 690 Krotkov, N. A., Lamsal, L. N., Celarier, E. A., Swartz, W. H., Marchenko, S. V., Bucsela, E. J., Chan, K. L., Wenig, M., and Zara, M.: The version 3 OMI NO₂ standard product, *Atmospheric Measurement Techniques*, 10, 3133–3149, <https://doi.org/10.5194/amt-10-3133-2017>, 2017.
- Kuhlmann, G., Hartl, A., Cheung, H. M., Lam, Y. F., and Wenig, M. O.: A novel gridding algorithm to create regional trace gas maps from satellite observations, *Atmospheric Measurement Techniques*, 7, 451–467, <https://doi.org/10.5194/amt-7-451-2014>, 2014.
- 695 Lapierre, J. L., Laughner, J. L., Geddes, J. A., Koshack, W., Cohen, R. C., and Pusede, S. E.: Observing regional variability in lightning NO_x production rates, *Journal of Geophysical Research*, in review, 2019.
- Lapierre, J. L., Laughner, J. L., Geddes, J. A., Koshack, W., Cohen, R. C., and Pusede, S. E.: Observing U.S. regional variability in lightning NO₂ production rates, *Journal of Geophysical Research: Atmospheres*, <https://doi.org/10.1029/2019JD031362>, 2020.
- Laughner, J. L. and Cohen, R. C.: Quantification of the effect of modeled lightning NO₂ on UV–visible air mass factors, *Atmospheric Measurement Techniques*, 10, 4403–4419, <https://doi.org/10.5194/amt-10-4403-2017>, 2017.
- 700 Laughner, J. L., Zhu, Q., and Cohen, R. C.: The Berkeley High Resolution Tropospheric NO₂ Product, *Earth System Science Data Discussions*, pp. 1–33, <https://doi.org/10.5194/essd-2018-66>, 2018a.
- Laughner, J. L., Zhu, Q., and Cohen, R. C.: Evaluation of version 3.0B of the BEHR OMI NO₂ product, *Atmospheric Measurement Techniques Discussions*, pp. 1–25, <https://doi.org/10.5194/amt-2018-248>, 2018b.
- 705 Laughner, J. L., Zhu, Q., and Cohen, R. C.: Evaluation of version 3.0B of the BEHR OMI NO₂ product, *Atmospheric Measurement Techniques*, 12, 129–146, <https://doi.org/10.5194/amt-12-129-2019>, 2019.
- Levelt, P. F., van den Oord, G., Dobber, M. R., Malkki, A., Visser, H., Vries, J. d., Stammes, P., Lundell, J., and Saari, H.: The ozone monitoring instrument, *IEEE Transactions on Geoscience and Remote Sensing*, 44, 1093–1101, <https://doi.org/10.1109/TGRS.2006.872333>, 2006.
- 710 Levelt, P. F., Joiner, J., Tamminen, J., Veefkind, J. P., Bhartia, P. K., Stein Zweers, D. C., Duncan, B. N., Streets, D. G., Eskes, H., van der A, R., McLinden, C., Fioletov, V., Carn, S., de Laat, J., DeLand, M., Marchenko, S., McPeters, R., Ziemke, J., Fu, D., Liu, X., Pickering, K., Apituley, A., González Abad, G., Arola, A., Boersma, F., Chan Miller, C., Chance, K., de Graaf, M., Hakkarainen, J., Hassinen, S., Ialongo, I., Kleipool, Q., Krotkov, N., Li, C., Lamsal, L., Newman, P., Nowlan, C., Suleiman, R., Tilstra, L. G., Torres, O., Wang, H.,

- and Wargan, K.: The Ozone Monitoring Instrument: overview of 14 years in space, *Atmospheric Chemistry and Physics*, 18, 5699–5745, <https://doi.org/10.5194/acp-18-5699-2018>, 2018.
- 715 Li, Y., Pickering, K. E., Allen, D. J., Barth, M. C., Bela, M. M., Cummings, K. A., Carey, L. D., Mecikalski, R. M., Fierro, A. O., Campos, T. L., Weinheimer, A. J., Diskin, G. S., and Biggerstaff, M. I.: Evaluation of deep convective transport in storms from different convective regimes during the DC3 field campaign using WRF-Chem with lightning data assimilation, *Journal of Geophysical Research: Atmospheres*, 122, 7140–7163, <https://doi.org/10.1002/2017JD026461>, 2017.
- 720 Li, Y., Pickering, K. E., Barth, M. C., Bela, M. M., Cummings, K. A., and Allen, D. J.: Evaluation of Parameterized Convective Transport of Trace Gases in Simulation of Storms Observed During the DC3 Field Campaign, *Journal of Geophysical Research: Atmospheres*, 123, 11,238–11,261, <https://doi.org/10.1029/2018JD028779>, 2018.
- Luo, C., Wang, Y., and Koshak, W. J.: Development of a self-consistent lightning NO_x simulation in large-scale 3-D models, *Journal of Geophysical Research: Atmospheres*, 122, 3141–3154, <https://doi.org/10.1002/2016JD026225>, 2017.
- 725 Marais, E. A., Jacob, D. J., Choi, S., Joiner, J., Belmonte-Rivas, M., Cohen, R. C., Beirle, S., Murray, L. T., Schiferl, L., Shah, V., and Jaeglé, L.: Nitrogen oxides in the global upper troposphere: interpreting cloud-sliced NO₂ observations from the OMI satellite instrument, *Atmospheric Chemistry and Physics Discussions*, pp. 1–14, <https://doi.org/10.5194/acp-2018-556>, 2018.
- Martin, R. V., Sauvage, B., Folkins, I., Sioris, C. E., Boone, C., Bernath, P., and Ziemke, J.: Space-based constraints on the production of nitric oxide by lightning, *Journal of Geophysical Research*, 112, 1479, <https://doi.org/10.1029/2006JD007831>, 2007.
- 730 McKinney, W.: pandas: a foundational Python library for data analysis and statistics, *Python for High Performance and Scientific Computing*, 14, 2011.
- Mecikalski, R. M. and Carey, L. D.: Lightning characteristics relative to radar, altitude and temperature for a multicell, MCS and supercell over northern Alabama, *Atmospheric Research*, 191, 128–140, <https://doi.org/10.1016/j.atmosres.2017.03.001>, <http://www.sciencedirect.com/science/article/pii/S0169809516302812>, 2017.
- 735 Met Office: Cartopy: a cartographic python library with a matplotlib interface, Exeter, Devon, <http://scitools.org.uk/cartopy>, 2010 - 2015.
- Min, M., Wu, C., Li, C., Liu, H., Xu, N., Wu, X., Chen, L., Wang, F., Sun, F., Qin, D., Wang, X., Li, B., Zheng, Z., Cao, G., and Dong, L.: Developing the science product algorithm testbed for Chinese next-generation geostationary meteorological satellites: Fengyun-4 series, *JOURNAL OF METEOROLOGICAL RESEARCH*, 31, 708–719, <https://doi.org/10.1007/s13351-017-6161-z>, 2017.
- Myhre, G., Shindell, D., Bréon, F. M., Collins, W., Fuglestedt, J., Huang, J., Koch, D., Lamarque, J. F., Lee, D., and Mendoza, B.: Climate change 2013: the physical science basis. Contribution of Working Group I to the Fifth Assessment Report of the Intergovernmental Panel on Climate Change, K., Tignor, M., Allen, SK, Boschung, J., Nauels, A., Xia, Y., Bex, V., and Midgley, PM, Cambridge University Press Cambridge, United Kingdom and New York, NY, USA, 2013.
- 740 Nault, B. A., Garland, C., Wooldridge, P. J., Brune, W. H., Campuzano-Jost, P., Crouse, J. D., Day, D. A., Dibb, J., Hall, S. R., Huey, L. G., Jimenez, J. L., Liu, X., Mao, J., Mikoviny, T., Peischl, J., Pollack, I. B., Ren, X., Ryerson, T. B., Scheuer, E., Ullmann, K., Wennberg, P. O., Wisthaler, A., Zhang, L., and Cohen, R. C.: Observational Constraints on the Oxidation of NO_x in the Upper Troposphere, *The Journal of Physical Chemistry A*, 120, 1468–1478, <https://doi.org/10.1021/acs.jpca.5b07824>, 2016.
- 745 Nault, B. A., Laughner, J. L., Wooldridge, P. J., Crouse, J. D., Dibb, J., Diskin, G., Peischl, J., Podolske, J. R., Pollack, I. B., Ryerson, T. B., Scheuer, E., Wennberg, P. O., and Cohen, R. C.: Lightning NO_x Emissions: Reconciling Measured and Modeled Estimates With Updated NO_x Chemistry, *Geophysical Research Letters*, 44, 9479–9488, <https://doi.org/10.1002/2017GL074436>, 2017.

- 750 Ott, L. E., Pickering, K. E., Stenchikov, G. L., Huntrieser, H., and Schumann, U.: Effects of lightning NO_x production during the 21 July European Lightning Nitrogen Oxides Project storm studied with a three-dimensional cloud-scale chemical transport model, *Journal of Geophysical Research*, 112, 61, <https://doi.org/10.1029/2006JD007365>, 2007.
- Ott, L. E., Pickering, K. E., Stenchikov, G. L., Allen, D. J., DeCaria, A. J., Ridley, B., Lin, R.-F., Lang, S., and Tao, W.-K.: Production of lightning NO_x and its vertical distribution calculated from three-dimensional cloud-scale chemical transport model simulations, *Journal of Geophysical Research*, 115, 4711, <https://doi.org/10.1029/2009JD011880>, 2010.
- 755 Pickering, K. E., Thompson, A. M., Wang, Y., Tao, W.-K., McNamara, D. P., Kirchhoff, V. W. J. H., Heikes, B. G., Sachse, G. W., Bradshaw, J. D., Gregory, G. L., and Blake, D. R.: Convective transport of biomass burning emissions over Brazil during TRACE A, *Journal of Geophysical Research*, 101, 23 993–24 012, <https://doi.org/10.1029/96JD00346>, 1996.
- Pickering, K. E., Bucsela, E., Allen, D., Ring, A., Holzworth, R., and Krotkov, N.: Estimates of lightning NO_x production
760 based on OMI NO₂ observations over the Gulf of Mexico, *Journal of Geophysical Research: Atmospheres*, 121, 8668–8691, <https://doi.org/10.1002/2015JD024179>, 2016.
- Platt, U. and Perner, D.: Measurements of Atmospheric Trace Gases by Long Path Differential UV/Visible Absorption Spectroscopy, in: *Optical and Laser Remote Sensing*, edited by Schawlow, A. L., Killinger, D. K., and Mooradian, A., vol. 39 of *Springer Series in Optical Sciences*, pp. 97–105, Springer Berlin Heidelberg, Berlin, Heidelberg, https://doi.org/10.1007/978-3-540-39552-2_13, 1983.
- 765 Price, C. and Rind, D.: A simple lightning parameterization for calculating global lightning distributions, *Journal of Geophysical Research*, 97, 9919–9933, <https://doi.org/10.1029/92JD00719>, 1992.
- Richter, A., Burrows, J. P., Nüß, H., Granier, C., and Niemeier, U.: Increase in tropospheric nitrogen dioxide over China observed from space, *Nature*, 437, 129–132, <https://doi.org/10.1038/nature04092>, 2005.
- Romps, D. M.: Evaluating the future of lightning in cloud-resolving models, *Geophysical Research Letters*,
770 <https://doi.org/10.1029/2019GL085748>, 2019.
- Romps, D. M., Seeley, J. T., Vollaro, and Molinari, J.: Projected increase in lightning strikes in the United States due to global warming, *Atmospheric Chemistry and Physics*, 346, 851–854, <https://doi.org/10.1126/science.1259100>, 2014.
- Rudlosky, S.: Evaluating ENTLN performance relative to TRMM/LIS, *Journal of Operational Meteorology*, 3, 11–20, <https://doi.org/10.15191/nwajom.2015.0302>, 2015.
- 775 Schaaf, C. B., Liu, J., Gao, F., and Strahler, A. H.: Aqua and Terra MODIS Albedo and Reflectance Anisotropy Products, in: *Land Remote Sensing and Global Environmental Change*, edited by Ramachandran, B., Justice, C. O., and Abrams, M. J., vol. 11 of *Remote Sensing and Digital Image Processing*, pp. 549–561, Springer New York, New York, NY, https://doi.org/10.1007/978-1-4419-6749-7_24, 2011.
- Schumann, U. and Huntrieser, H.: The global lightning-induced nitrogen oxides source, *Atmospheric Chemistry and Physics*, 7, 3823–3907, <https://doi.org/10.5194/acp-7-3823-2007>, 2007.
- 780 Schwantes, R. H., Teng, A. P., Nguyen, T. B., Coggon, M. M., Crouse, J. D., St Clair, J. M., Zhang, X., Schilling, K. A., Seinfeld, J. H., and Wennberg, P. O.: Isoprene NO₃ Oxidation Products from the RO₂ + HO₂ Pathway, *The Journal of Physical Chemistry A*, 119, 10 158–10 171, <https://doi.org/10.1021/acs.jpca.5b06355>, 2015.
- Seabold, S. and Perktold, J.: statsmodels: Econometric and statistical modeling with python, in: 9th Python in Science Conference, 2010.
- Silvern, R. F., Jacob, D. J., Travis, K. R., Sherwen, T., Evans, M. J., Cohen, R. C., Laughner, J. L., Hall, S. R., Ullmann, K., Crouse, J. D.,
785 Wennberg, P. O., Peischl, J., and Pollack, I. B.: Observed NO/NO₂ ratios in the upper troposphere imply errors in NO-NO₂-O₃ cycling kinetics or an unaccounted NO_x reservoir, *Geophysical Research Letters*, <https://doi.org/10.1029/2018GL077728>, 2018.

- Sneep, M., de Haan, J. F., Stammes, P., Wang, P., Vanbauce, C., Joiner, J., Vasilkov, A. P., and Levelt, P. F.: Three-way comparison between OMI and PARASOL cloud pressure products, *Journal of Geophysical Research*, 113, D05 204, <https://doi.org/10.1029/2007JD008694>, 2008.
- 790 Stammes, P., Sneep, M., de Haan, J. F., Veefkind, J. P., Wang, P., and Levelt, P. F.: Effective cloud fractions from the Ozone Monitoring Instrument: Theoretical framework and validation, *Journal of Geophysical Research*, 113, D05 204, <https://doi.org/10.1029/2007JD008820>, 2008.
- Strode, S. A., Douglass, A. R., Ziemke, J. R., Manyin, M., Nielsen, J. E., and Oman, L. D.: A Model and Satellite-Based Analysis of the Tropospheric Ozone Distribution in Clear Versus Convectively Cloudy Conditions, *Journal of Geophysical Research: Atmospheres*, 122, 11,948–11,960, <https://doi.org/10.1002/2017JD027015>, 2017.
- 795 Travis, K. R., Jacob, D. J., Fisher, J. A., Kim, P. S., Marais, E. A., Zhu, L., Yu, K., Miller, C. C., Yantosca, R. M., Sulprizio, M. P., Thompson, A. M., Wennberg, P. O., Crouse, J. D., St Clair, J. M., Cohen, R. C., Laughner, J. L., Dibb, J. E., Hall, S. R., Ullmann, K., Wolfe, G. M., Pollack, I. B., Peischl, J., Neuman, J. A., and Zhou, X.: Why do Models Overestimate Surface Ozone in the Southeastern United States?, *Atmospheric Chemistry and Physics*, 16, 13 561–13 577, <https://doi.org/10.5194/acp-16-13561-2016>, 2016.
- 800 van der Walt, S., Colbert, S. C., and Varoquaux, G.: The NumPy Array: A Structure for Efficient Numerical Computation, *Computing in Science & Engineering*, 13, 22–30, <https://doi.org/10.1109/MCSE.2011.37>, 2011.
- Vasilkov, A., Joiner, J., Spurr, R., Bhartia, P. K., Levelt, P., and Stephens, G.: Evaluation of the OMI cloud pressures derived from rotational Raman scattering by comparisons with other satellite data and radiative transfer simulations, *Journal of Geophysical Research*, 113, D05 204, <https://doi.org/10.1029/2007JD008689>, 2008.
- 805 Veefkind, J. P., Aben, I., McMullan, K., Förster, H., de Vries, J., Otter, G., Claas, J., Eskes, H. J., de Haan, J. F., Kleipool, Q., van Weele, M., Hasekamp, O., Hoogeveen, R., Landgraf, J., Snel, R., Tol, P., Ingmann, P., Voors, R., Kruizinga, B., Vink, R., Visser, H., and Levelt, P. F.: TROPOMI on the ESA Sentinel-5 Precursor: A GMES mission for global observations of the atmospheric composition for climate, air quality and ozone layer applications, *Remote Sensing of Environment*, 120, 70–83, <https://doi.org/10.1016/j.rse.2011.09.027>, 2012.
- Wang, L., Follette-Cook, M. B., Newchurch, M. J., Pickering, K. E., Pour-Biazar, A., Kuang, S., Koshak, W., and Peterson, H.: Evaluation of lightning-induced tropospheric ozone enhancements observed by ozone lidar and simulated by WRF/Chem, *Atmospheric Environment*, 115, 185–191, <https://doi.org/10.1016/j.atmosenv.2015.05.054>, 2015.
- 810 Waskom, M., Botvinnik, O., O’Kane, D., Hobson, P., Lukauskas, S., Gemperline, D. C., Augspurger, T., Halchenko, Y., Cole, J. B., Warmenhoven, J., de Ruiter, J., Pye, C., Hoyer, S., Vanderplas, J., Villalba, S., Kunter, G., Quintero, E., Bachant, P., Martin, M., Meyer, K., Miles, A., Ram, Y., Yarkoni, T., Williams, M. L., Evans, C., Fitzgerald, C., Brian, F., Fonesbeck, C., Lee, A., and Qalieh, A.: Mwaskom/Seaborn: V0.8.1 (September 2017), <https://doi.org/10.5281/zenodo.883859>, 2017.
- Williams, E. R.: The tripole structure of thunderstorms, *Journal of Geophysical Research*, 94, 13 151, <https://doi.org/10.1029/JD094iD11p13151>, 1989.
- Wong, J., Barth, M. C., and Noone, D.: Evaluating a lightning parameterization based on cloud-top height for mesoscale numerical model simulations, *Geoscientific Model Development*, 6, 429–443, <https://doi.org/10.5194/gmd-6-429-2013>, 2013.
- 820 Xu, K.-M. and Randall, D. A.: A Semiempirical Cloudiness Parameterization for Use in Climate Models, *Journal of the Atmospheric Sciences*, 53, 3084–3102, [https://doi.org/10.1175/1520-0469\(1996\)053<3084:ASCPFU>2.0.CO;2](https://doi.org/10.1175/1520-0469(1996)053<3084:ASCPFU>2.0.CO;2), 1996.
- Yang, J., Zhang, Z., Wei, C., Lu, F., and Guo, Q.: Introducing the New Generation of Chinese Geostationary Weather Satellites, Fengyun-4, *Bulletin of the American Meteorological Society*, 98, 1637–1658, <https://doi.org/10.1175/BAMS-D-16-0065.1>, 2017.

- Zel'dovich, Y. and Raizer, Y.: VIII - Physical and chemical kinetics in hydrodynamic processes, in: *Physics of Shock Waves and High-Temperature Hydrodynamic Phenomena*, edited by Hayes, W. D., Probstein, R. F., Zel'dovich, Y., and Raizer, Y., pp. 566–571, Academic Press, <https://doi.org/10.1016/B978-0-12-395672-9.50009-6>, 1967.
- Zhang, P., Lu, Q., Hu, X., Gu, S., Yang, L., Min, M., Chen, L., Xu, N., Sun, L., Bai, W., Ma, G., and Di Xian: Latest Progress of the Chinese Meteorological Satellite Program and Core Data Processing Technologies, *Advances in Atmospheric Sciences*, 36, 1027–1045, <https://doi.org/10.1007/s00376-019-8215-x>, 2019.
- 825 Zhang, X. and Laughner, J.: zxdawn/BEHR-LNOx: v1.0, Zenodo, <https://doi.org/10.5281/zenodo.3553426>, 2019.
- Zhao, C., Wang, Y., Choi, Y., and Zeng, T.: Summertime impact of convective transport and lightning NO_x production over North America: modeling dependence on meteorological simulations, *Atmospheric Chemistry and Physics*, 9, 4315–4327, <https://doi.org/10.5194/acp-9-4315-2009>, 2009.
- Zhou, Y., Brunner, D., Boersma, K. F., Dirksen, R., and Wang, P.: An improved tropospheric NO₂ retrieval for OMI observations in the vicinity of mountainous terrain, *Atmospheric Measurement Techniques*, 2, 401–416, <https://doi.org/10.5194/amt-2-401-2009>, 2009.
- 835 Zhu, Q., Laughner, J. L., and Cohen, R. C.: Lightning NO₂ simulation over the contiguous US and its effects on satellite NO₂ retrievals, *Atmospheric Chemistry and Physics*, 19, 13 067–13 078, <https://doi.org/10.5194/acp-19-13067-2019>, 2019.
- Zhu, Y., Rakov, V. A., Tran, M. D., and Nag, A.: A study of National Lightning Detection Network responses to natural lightning based on ground truth data acquired at LOG with emphasis on cloud discharge activity, *Journal of Geophysical Research: Atmospheres*, 121, 14,651–14,660, <https://doi.org/10.1002/2016JD025574>, 2016.
- 840 Zhu, Y., Rakov, V. A., Tran, M. D., Stock, M. G., Heckman, S., Liu, C., Sloop, C. D., Jordan, D. M., Uman, M. A., Caicedo, J. A., Kotovsky, D. A., Wilkes, R. A., Carvalho, F. L., Ngin, T., Gamerota, W. R., Pilkey, J. T., and Hare, B. M.: Evaluation of ENTLN Performance Characteristics Based on the Ground Truth Natural and Rocket-Triggered Lightning Data Acquired in Florida, *Journal of Geophysical Research: Atmospheres*, 122, 9858–9866, <https://doi.org/10.1002/2017JD027270>, 2017.
- 845 Ziemke, J. R., Joiner, J., Chandra, S., Bhartia, P. K., Vasilkov, A., Haffner, D. P., Yang, K., Schoeberl, M. R., Froidevaux, L., and Levelt, P. F.: Ozone mixing ratios inside tropical deep convective clouds from OMI satellite measurements, *Atmospheric Chemistry and Physics*, 9, 573–583, <https://doi.org/10.5194/acp-9-573-2009>, 2009.
- Ziemke, J. R., Strode, S. A., Douglass, A. R., Joiner, J., Vasilkov, A., Oman, L. D., Liu, J., Strahan, S. E., Bhartia, P. K., and Haffner, D. P.: A cloud-ozone data product from Aura OMI and MLS satellite measurements, *Atmospheric Measurement Techniques*, 10, 4067–4078, <https://doi.org/10.5194/amt-10-4067-2017>, 2017.
- 850

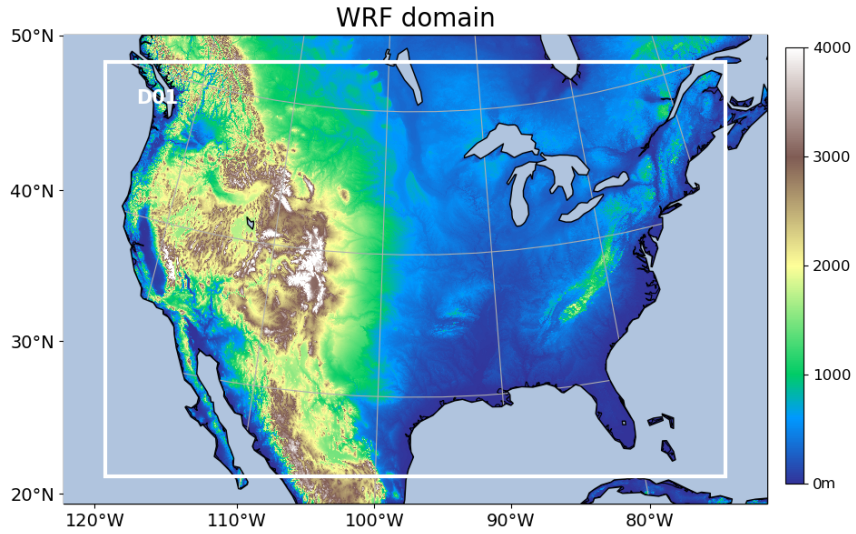


Figure 1. Domain and terrain height (m) of the WRF-Chem simulation with 350 x 290 grid cells and a horizontal resolution of 12 km.

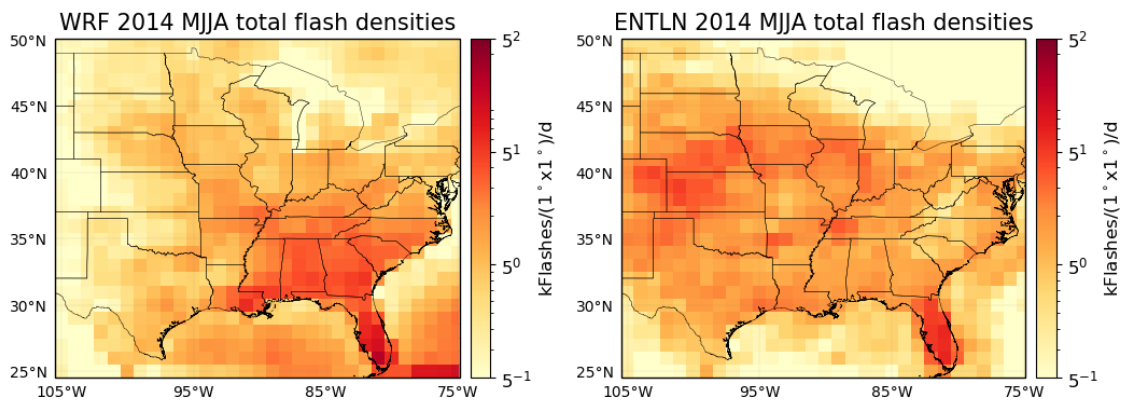


Figure 2. Comparison between total flash densities from ENTLN and WRF-Chem during MJJA 2014.

Table 1. Definitions of the abbreviations for the criteria used in this study.

Abbreviations	Full form [source]
CRF	Cloud radiance fraction [OMI]
CP	Cloud optical pressure [OMI]
CF	Cloud fraction [WRF-Chem]
TL	Total lightning flashes [WRF-Chem]
ratio	modeled LNO ₂ Vis / modeled NO ₂ Vis [WRF-Chem]
CRF _α _ENTLN	CRF ≥ α + ENTLN flashes(strokes) ≥ 2400(8160) [ENTLN]
CRF _α _CF40_ENTLN	CRF ≥ α + ENTLN flashes(strokes) ≥ 2400(8160) + CF ≥ 40%
CRF _α _ENTLN_TL1000	CRF ≥ α + ENTLN flashes(strokes) ≥ 2400(8160) + TL ≥ 1000
CRF _α _CF40_ENTLN_TL1000	CRF ≥ α + ENTLN flashes(strokes) ≥ 2400(8160) + CF ≥ 40% + TL ≥ 1000
CRF _α _ENTLN_TL1000_ratio50	CRF ≥ α + ENTLN flashes(strokes) ≥ 2400(8160) + TL ≥ 1000 + ratio ≥ 50%
CRF _α _CF40_ENTLN_TL1000_ratio50	CRF ≥ α + ENTLN flashes(strokes) ≥ 2400(8160) + CF ≥ 40% + TL ≥ 1000 + ratio ≥ 50%
<u>CRF_α_ENTLN(3.4)_TL1_ratio50</u>	<u>CRF ≥ α + ENTLN flashes(strokes) ≥ 1(3.4) + TL ≥ 1 + ratio ≥ 50%</u>

α has three options: 70%, 90% and 100%

Table 2. LNO_x production [efficiencies](#) for different combinations of criteria defined in Table 1.

Condition ¹	ENTLN data type ²	LNO _x /flash or LNO _x /stroke	R value	Intercept (10 ⁶ mol)	Days ³
CRF90_ENTLN	Flash	52.1 ± 51.1	0.20	0.21	99
CRF90_CF40_ENTLN	Flash	84.2 ± 31.5	0.54	-0.04	70
CRF90_ENTLN_TL1000	Flash	61.9 ± 49.1	0.27	0.33	83
CRF90_CF40_ENTLN_TL1000	Flash	63.4 ± 52.9	0.38	0.26	38
CRF90_ENTLN_TL1000_ratio50	Flash	54.5 ± 48.1	0.25	0.39	81
CRF90_CF40_ENTLN_TL1000_ratio50	Flash	90.0 ± 65.0	0.46	0.15	32
CRF90_ENTLN	Stroke	6.7 ± 4.1	0.31	0.23	102
CRF90_CF40_ENTLN	Stroke	10.3 ± 3.6	0.55	0.08	79
CRF90_ENTLN_TL1000	Stroke	7.5 ± 5.1	0.29	0.38	94
CRF90_CF40_ENTLN_TL1000	Stroke	8.6 ± 6.2	0.39	0.27	46
CRF90_ENTLN_TL1000_ratio50	Stroke	7.0 ± 4.8	0.29	0.42	93
CRF90_CF40_ENTLN_TL1000_ratio50	Stroke	8.9 ± 7.0	0.39	0.31	40

¹These conditions are defined in Table 1. ²The thresholds of ENTLN data are 2400 flashes box⁻¹ and 8160 strokes box⁻¹ during the period of 2.4 h before OMI overpass time. ³The number of valid days with specific criteria in MJJA 2014.

Table 3. LNO_x production efficiencies for different thresholds of CRF with coincident ENTLN data, $TL \geq 1000$ and ratio $\geq 50\%$.

CRF (%)	ENTLN data type ¹	LNO_x /flash or LNO_x /stroke	R value	Intercept (10^5 mol)	Days ²
70	Flash	35.7 ± 36.8	0.21	4.91	85
90	Flash	54.5 ± 48.1	0.25	3.90	81
100	Flash	20.8 ± 37.4	0.13	5.67	71
70	Stroke	4.1 ± 3.9	0.21	5.16	96
90	Stroke	7.0 ± 4.8	0.29	4.16	93
100	Stroke	2.6 ± 4.0	0.14	5.41	82

¹The thresholds of ENTLN data are 2400 flashes box^{-1} and 8160 strokes box^{-1} during the period of 2.4 h before OMI overpass time. ²The number of valid days with specific criteria in MJJA 2014.

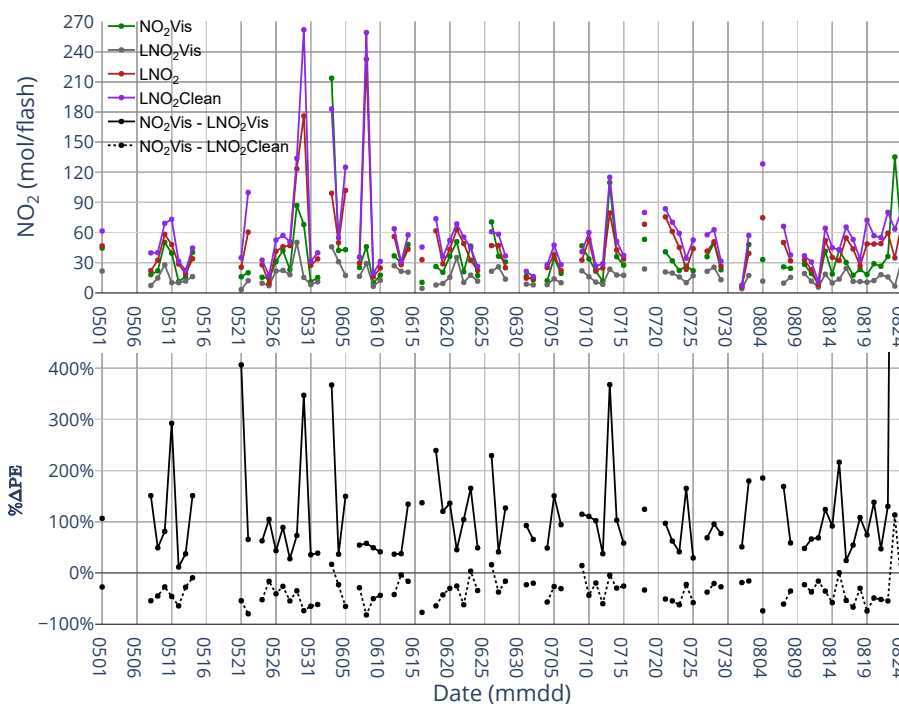


Figure 3. (top) Time series of NO_2 Vis, LNO_2 Vis, LNO_2 and LNO_2 Clean production per day over the CONUS for MJJA 2014 with CRF $\geq 90\%$ and a flash threshold of 2400 flashes per 2.4 h. (bottom) Time series of the percent differences between NO_2 Vis and LNO_2 Vis and the percent differences between NO_2 Vis and LNO_2 Clean with CRF $\geq 90\%$. The value of black dot on August 23 (not shown) is 1958%.

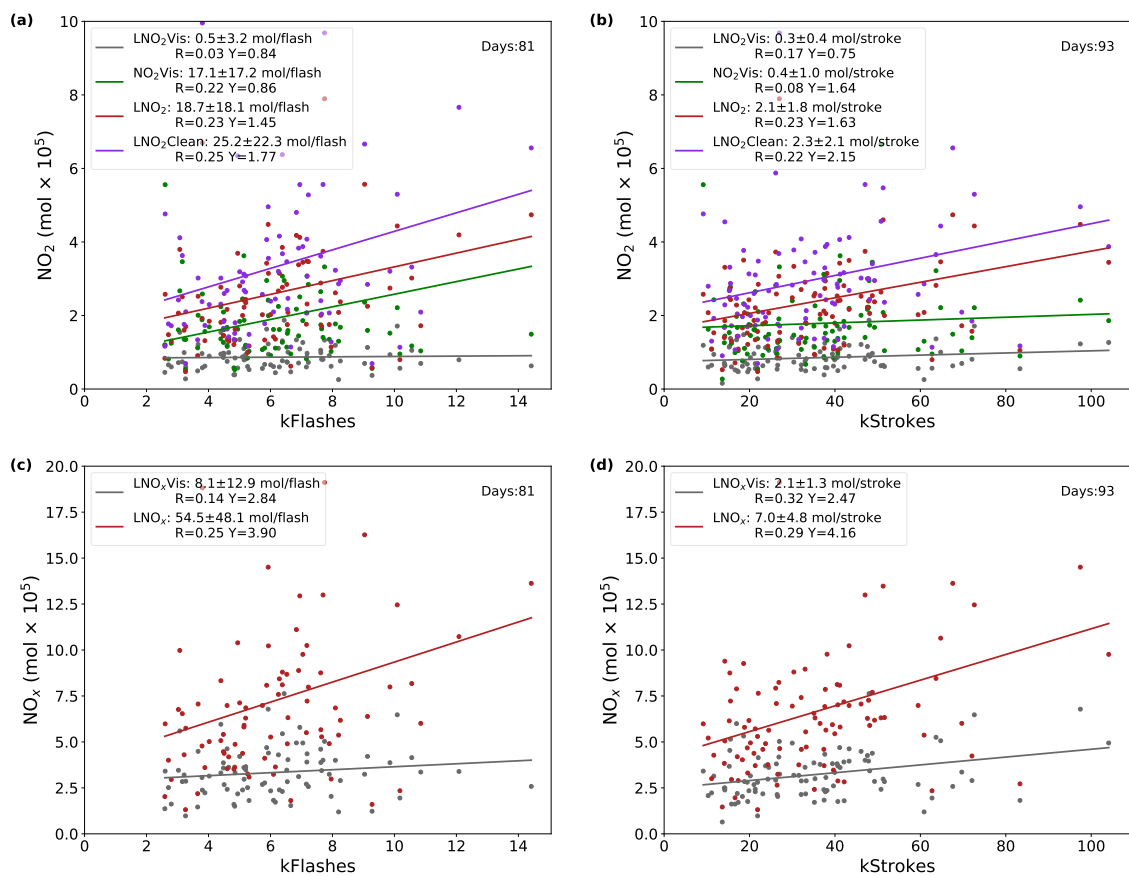


Figure 4. (a) Daily NO_2Vis , LNO_2Vis , LNO_2 and LNO_2Clean versus ENTLN total flashes data. (b) Same as (a) but for strokes. (c) Daily LNO_xVis and LNO_x versus total flashes. (d) Same as (c) but for strokes.

Table 4. The percent change changes in the estimated production when using different methods based on the same a priori profiles.

	City ¹	$(\text{LNO}_2\text{Clean} - \text{LNO}_2)/\text{LNO}_2$	$(\text{LNO}_2 - \text{TropVis})/\text{TropVis}$	$(\text{LNO}_2\text{Clean} - \text{TropVis})/\text{TropVis}$
Polluted	Lansing	24.2%	49.5%	85.6%
	New Orleans	13.3%	121.2%	153.8%
	Orlando	46.3%	37.5%	101.3%
Clean	Huron	12.0%	56.4%	75.2%
	Charles Town	12.0%	82.2%	104.1%
	Tarboro	5.0%	86.0%	95.3%

¹ Locations are denoted in Fig. 6a.

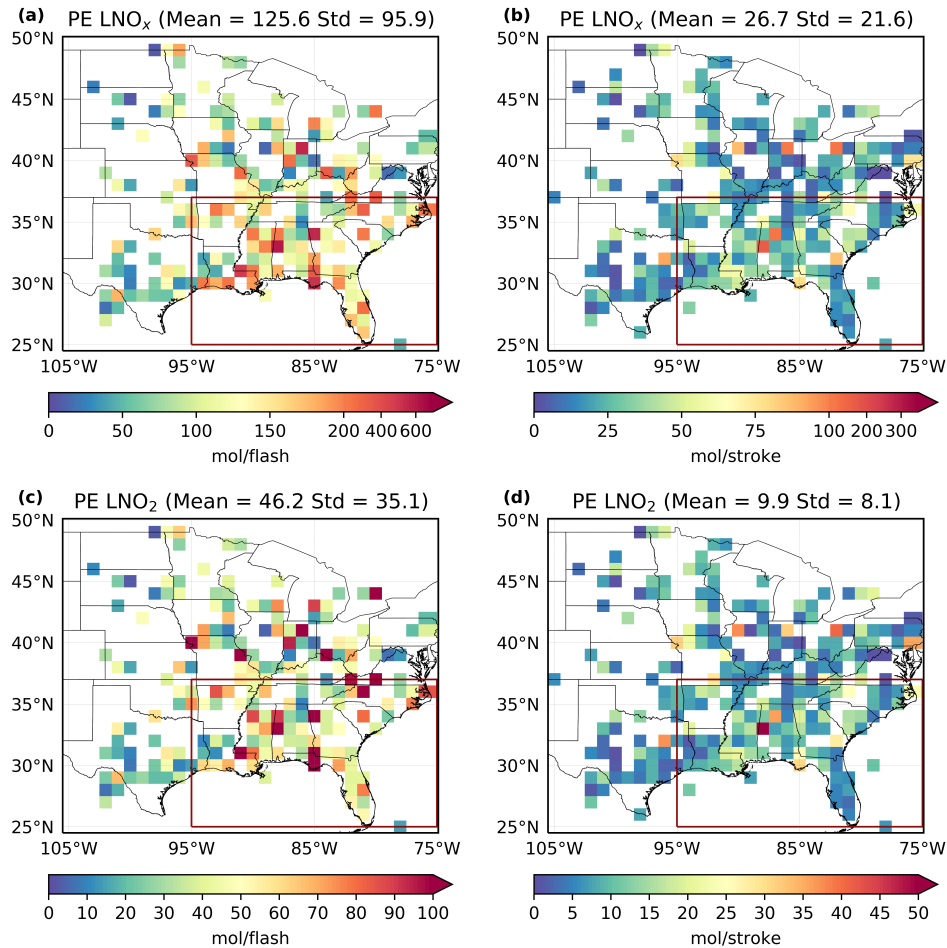


Figure 5. (a) and (c) Maps of $1^\circ \times 1^\circ$ gridded values of mean LNO_x and LNO₂ production per flash with CRF $\geq 90\%$ for MJJA 2014. (b) and (d) Same as (a) and (c) except for strokes. The southeastern US is denoted by the red box in panels a – d.

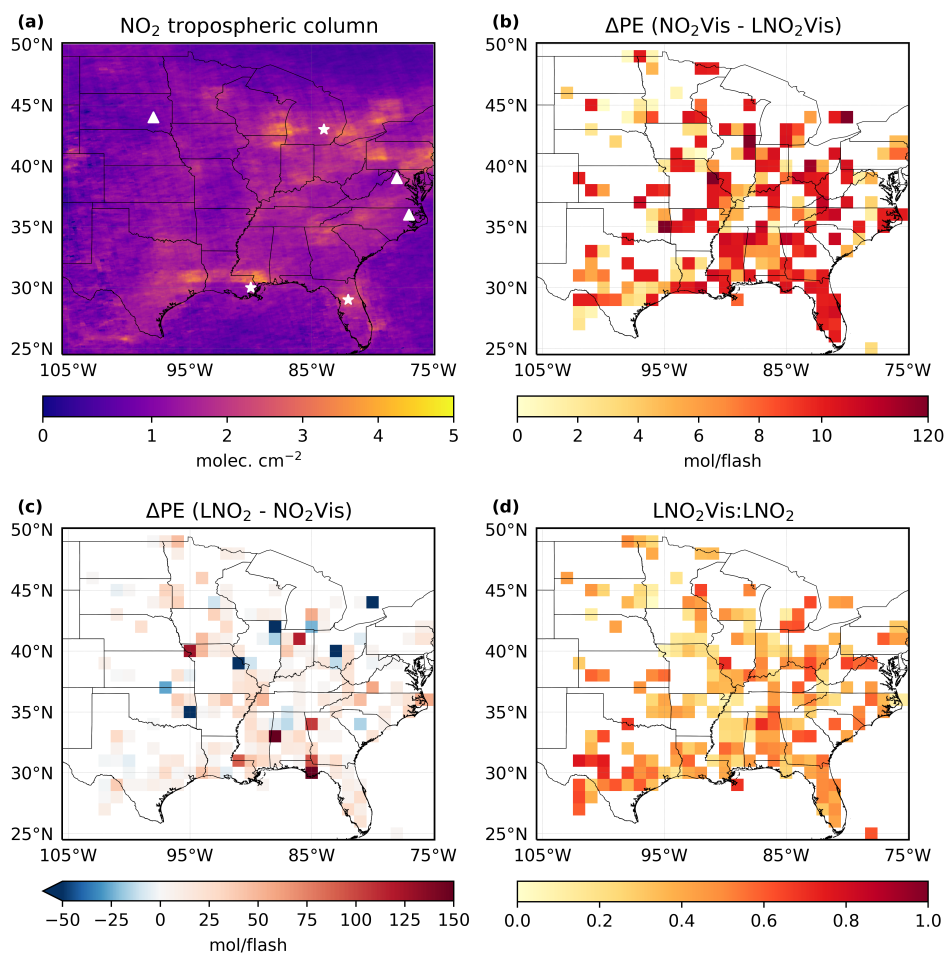


Figure 6. (a) Mean (MJJA 2014) NO₂ tropospheric column. Polluted cities are denoted by stars: Lansing, New Orleans and Orlando while clean cities are denoted by triangles: Huron, Charles Town and Tarboro. (b) The differences of the estimated mean production efficiency between NO₂Vis and LNO₂Vis with CRF ≥ 90%. (c) The same differences as (b) but between LNO₂ and NO₂Vis. (d) The ratio of LNO₂Vis to LNO₂.

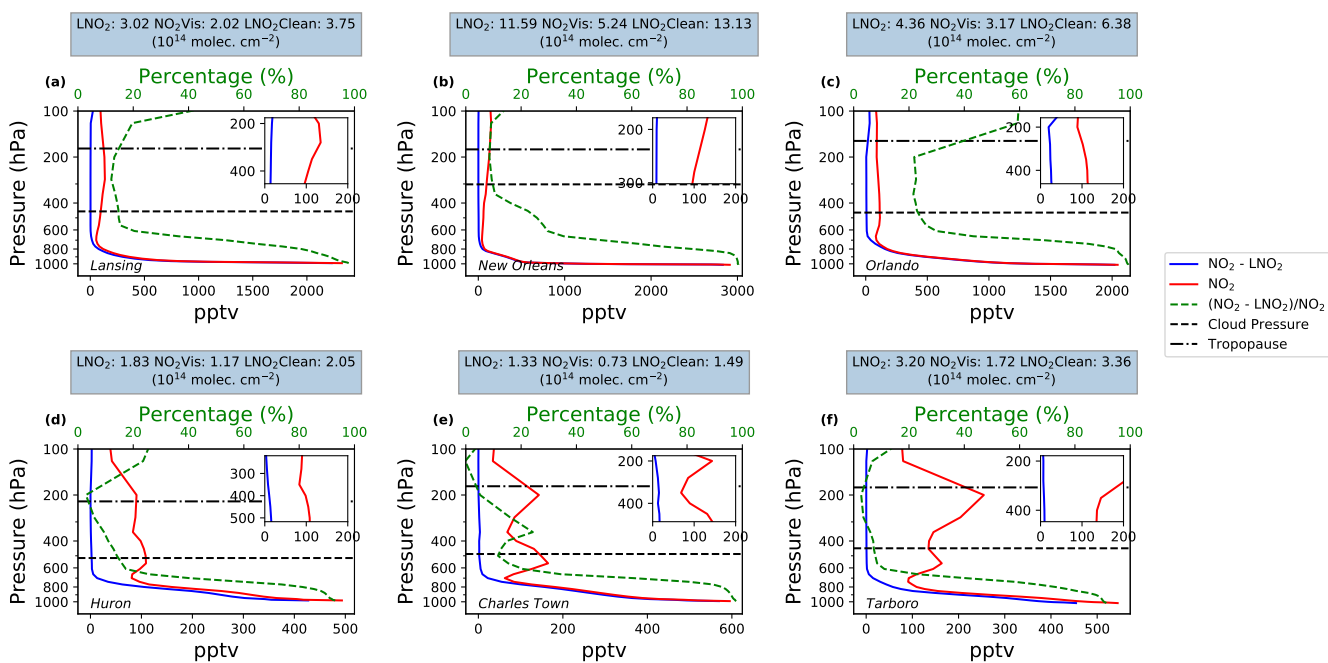


Figure 7. Comparison Comparisons of mean WRF-Chem NO_2 and background NO_2 profiles in six grids with $\text{CRF} \geq 100\%$ on specific days during MJJA 2014. The top row data are selected from polluted regions (stars in Fig. 6a) while the bottom row data are from clean regions (triangles in Fig. 6a). The green dashed lines are the mean ratio profiles of background NO_2 to total NO_2 . The zoomed figures show the profiles from the cloud pressure to the tropopause. The titles present the mean productions based on three different methods mentioned in Sect. 2.4.

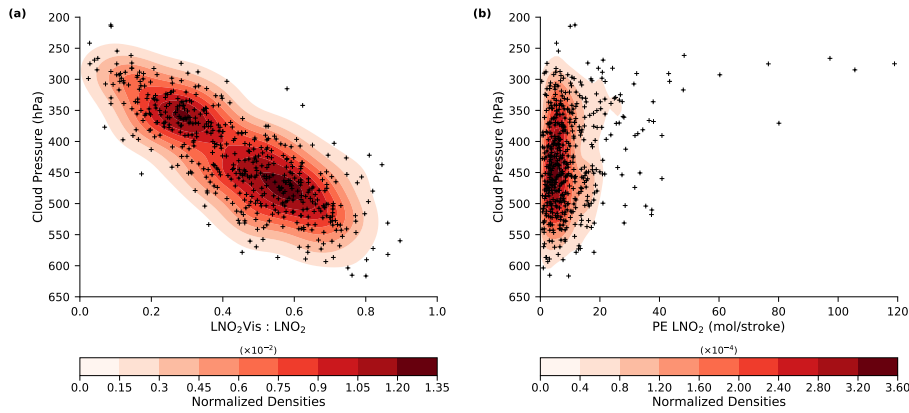


Figure 8. Kernel density estimation of the (a) daily ratio of LNO₂Vis to LNO₂ and (b) daily LNO₂ production efficiency versus the daily cloud pressure measured by OMI with CRF $\geq 90\%$ for MJJA 2014. [The kernel density estimation was generated by kdeplot in the Python package named seaborn.](#)

Table 5. Uncertainties for the estimation of LNO₂/flash, LNO_x/flash, LNO₂/stroke and LNO_x/stroke.

Type	Perturbation	LNO ₂ /flash ⁵	LNO _x /flash ⁵	LNO ₂ /stroke ⁵	LNO _x /stroke ⁵
BEHR tropopause pressure ¹	NASA product tropopause	6	4	6	4
Cloud radiance fraction ¹	$\pm 5\%$	2	2	2	2
Cloud pressure ²	Constant AMF: 0.46 Variable	23-32	23-34	23-32	23-34
Surface pressure ¹	$\pm 1.5\%$	0	0	0	0
Surface reflectivity ¹	$\pm 17\%$	0	0	0	0
LNO ₂ profile ¹	$2 \times 500 \text{ mol NO flash}^{-1}$	15-13	29-25	14-13	29-25
Profile location ¹	Quasi-Monte Carlo	0	1	0	1
Lightning detection efficiency ³	IC: $\pm 16\%$, CG: $\pm 5\%$	15	15	15	15
t_{window} ³	2 – 4 hours	10	10	8	8
LNO _x lifetime ³	2 – 12 hours	24	24	24	24
V_{strat} ⁴	-	10	10	10	10
Systematic errors in slant column ⁴	-	5	5	5	5
Tropospheric background ⁴	-	10	10	10	10
NO/NO ₂ ⁴	-20% \pm 15%	20-0	20-15	20-0	15
Net	-	48-49	54-56	47-48	54-56

PE_{uncertainty} = (Error_{rising perturbed value} - Error_{lowering perturbed value})/2 where Error perturbed value = (PE perturbed value - PE_{original value})/PE_{original value}.

¹Laughner et al. (2019) ²Acarreta et al. (2004) ³Lapierre et al. (2020) ⁴Allen et al. (2019) and Bucsele et al. (2019) ⁵Uncertainty (%)

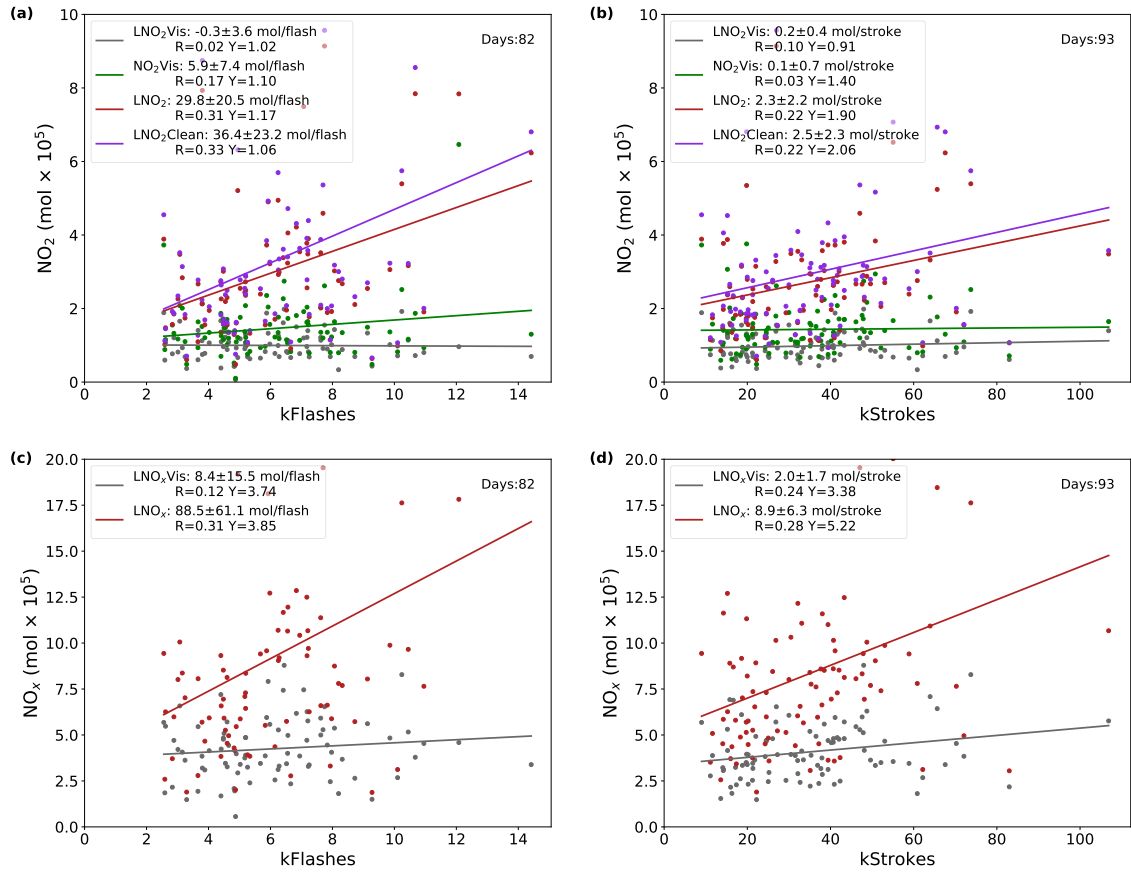


Figure 9. Same as Fig. 4 except for the 2×500 mol NO flash⁻¹ configuration.

Table A1. Simple forms of abbreviations for AMFs.

Abbreviations	Numerator ¹	Denominator ²
AMF _{LNO₂}	S _{NO₂}	V _{LNO₂}
AMF _{LNO₂Vis}	S _{NO₂}	V _{LNO₂Vis}
AMF _{LNO₂Clean}	S _{LNO₂}	V _{LNO₂}
AMF _{NO₂Vis}	S _{NO₂}	V _{NO₂Vis}
AMF _{LNO_x}	S _{NO₂}	V _{LNO_x}
AMF _{NO_xVis}	S _{NO₂}	V _{NO_xVis}

¹The part of simulated VCD seen by OMI ²The simulated VCD

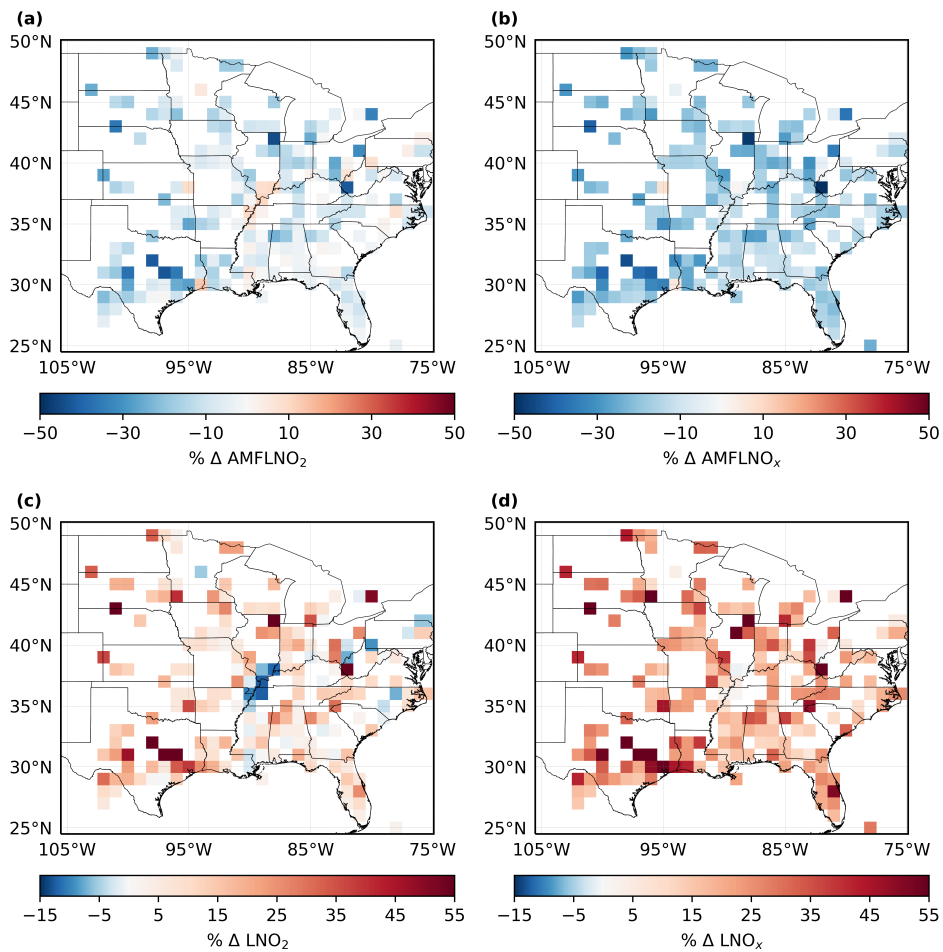


Figure 10. Average percent difference-differences in (a) $AMFLNO_2$, (b) $AMFLNO_x$, (c) LNO_2 and (d) LNO_x with $CRF \geq 90\%$ over MJJA 2014. Difference-Differences between profiles are generated by $2 \times 500 \text{ mol NO flash}^{-1}$ and $1 \times 200 \text{ mol NO flash}^{-1}$.

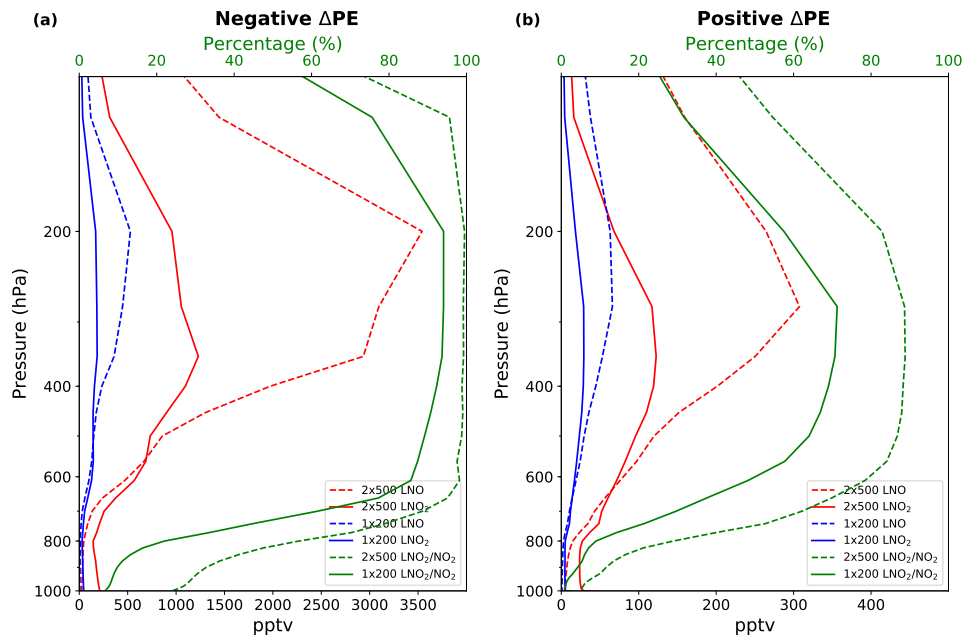


Figure 11. LNO and LNO₂ profiles with different LNO settings at (a) the region containing the minimal negative percent change in LNO₂ and (b) the region containing the largest positive percent change in LNO₂ when the LNO setting is changed from 1×200 mol NO flash⁻¹ to 2×500 mol NO flash⁻¹, averaged over MJJA 2014. The profiles using 1×200 (2×500) mol NO flash⁻¹ are shown in blue (red) lines. Solid (dashed) green lines are the mean ratio of LNO₂ to NO₂ with 1×200 (2×500) mol NO flash⁻¹.

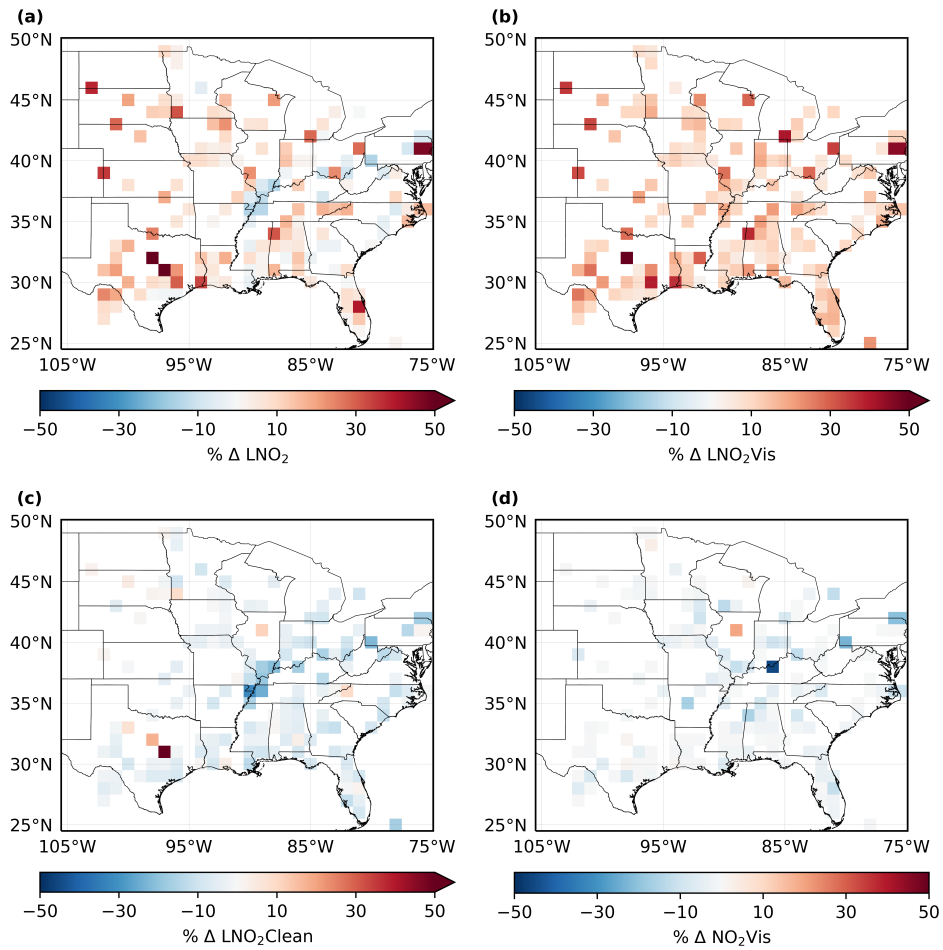


Figure 12. Average percent difference-differences in (a) LNO_2 , (b) $\text{LNO}_2 \text{Vis}$, (c) $\text{LNO}_2 \text{Clean}$ and (d) $\text{NO}_2 \text{Vis}$ with $\text{CRF} = 100\%$ over MJJA 2014.

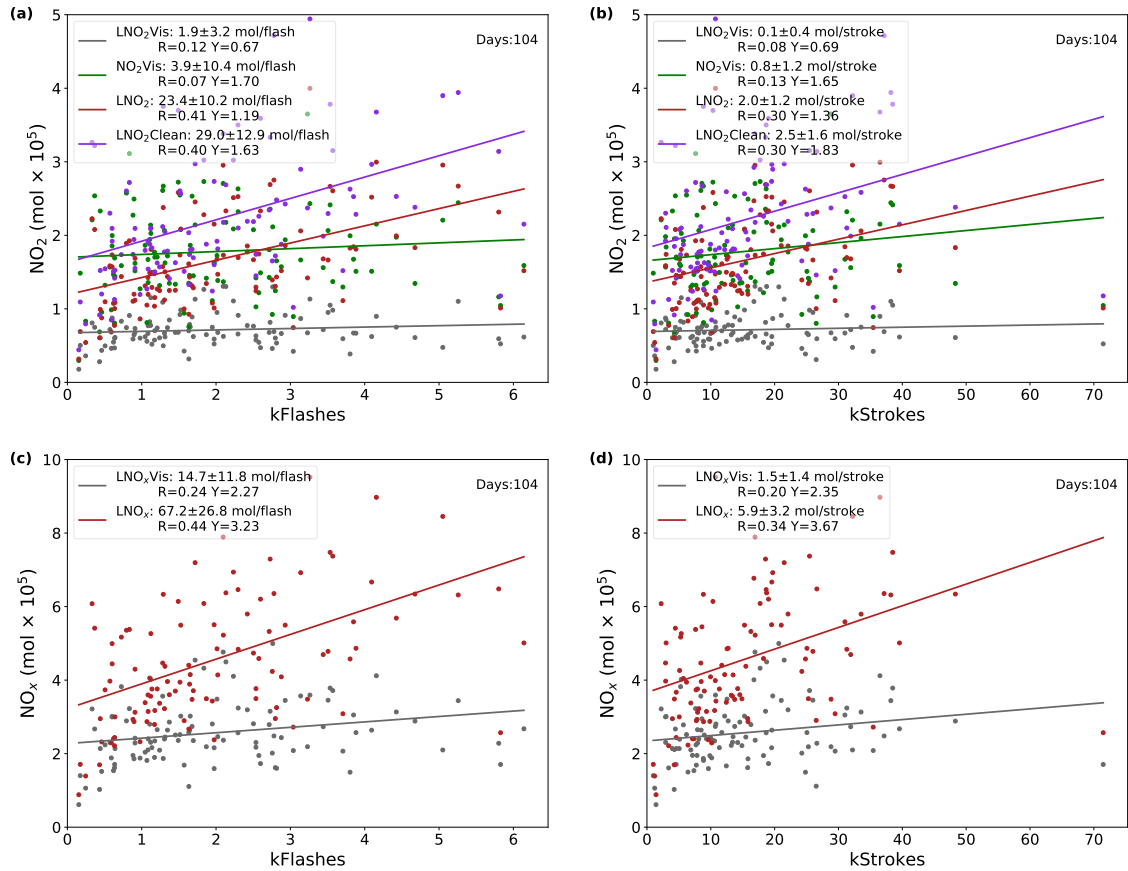


Figure B1. Linear regressions with CRF > 90% and a flash threshold of 1 flash box⁻¹ or 3.4 strokes box⁻¹ per 2.4 h. (a) Daily NO₂Vis, LNO₂Vis, LNO₂ and LNO₂Clean versus ENTLN total flashes data. (b) Same as (a) but for strokes. (c) Daily LNO_xVis and LNO_x versus total flashes. (d) Same as (c) but for strokes.

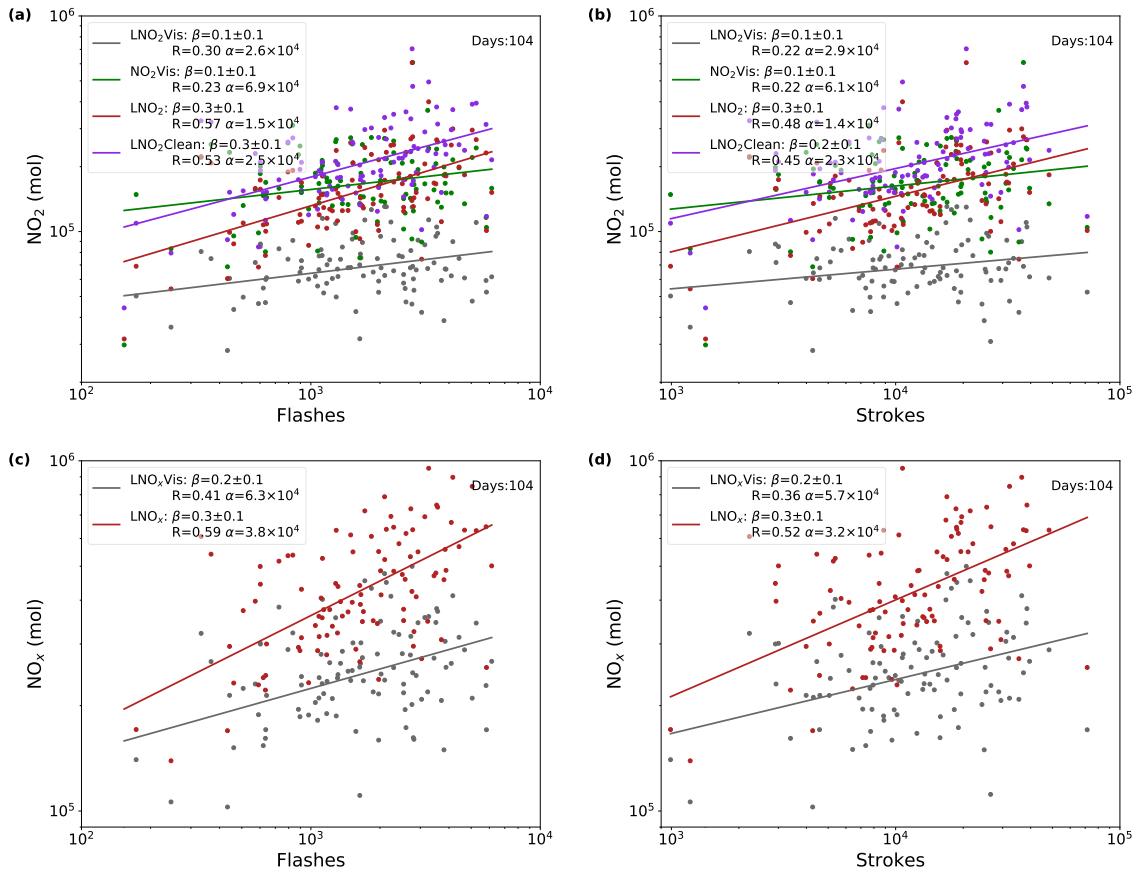


Figure B2. Same as Fig. B1 but using log-log axes.

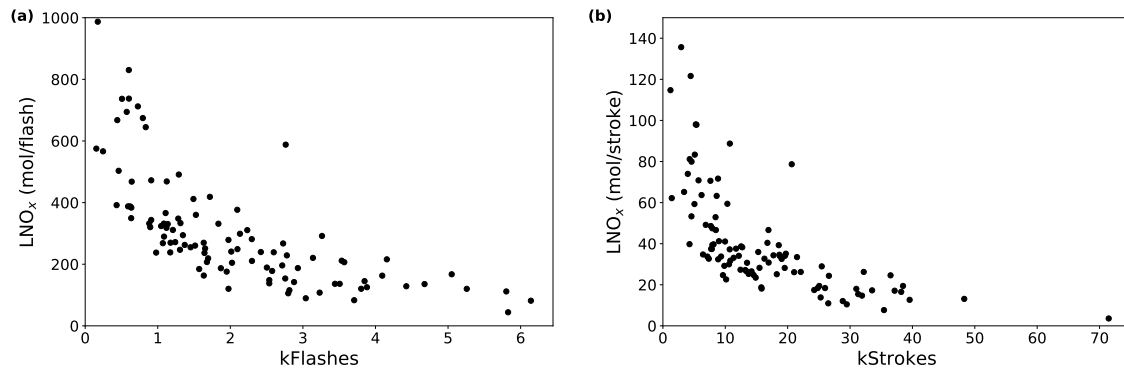


Figure B3. (a) Daily LNO_x production efficiencies versus ENTLN total flashes data, with CRF $\geq 90\%$ and a flash threshold of 1 flash box⁻¹.
 (b) Same as (a) but for strokes.